Separation & Purification Reviews
Publication details, including instructions for authors and subscription information:
http://www.informaworld.com/smpp/title~content=t713597294

Membrane Distillation and Related Operations—A Review

Efrem Curcio[ab]; Enrico Drioli[ab]
[a] Department of Chemical Engineering and Materials, University of Calabria, Italy [b] Institute on Membrane Technology ITM-CNR, University of Calabria, Italy

To cite this Article Curcio, Efrem and Drioli, Enrico(2005) 'Membrane Distillation and Related Operations—A Review', Separation & Purification Reviews, 34: 1, 35 — 86
To link to this Article: DOI: 10.1081/SPM-200054951
URL: http://dx.doi.org/10.1081/SPM-200054951

Separation and Purification Reviews, 34: 35–86, 2005

ISSN 1542-2119 print/1542-2127 online
DOI: 10.1081/SPM-200054951

Taylor & Francis
Taylor & Francis Group

Membrane Distillation and Related Operations—A Review

Efrem Curcio and Enrico Drioli
University of Calabria, Department of Chemical Engineering and Materials, Italy and Institute on Membrane Technology ITM-CNR, University of Calabria, Italy

Abstract: Membrane contactors represent an emerging technology in which the membrane is used as a tool for inter phase mass transfer operations: the membrane does not act as a selective barrier, but the separation is based on the phase equilibrium. In principle, all traditional stripping, scrubbing, absorption, evaporation, distillation, crystallization, emulsification, liquid-liquid extraction, and mass transfer catalysis processes can be carried out according to this configuration. This review, specifically addressed to membrane distillation (MD), osmotic distillation (OD), and membrane crystallization (MCr), illustrates the fundamental concepts related to heat and mass transport phenomena through microporous membranes, appropriate membrane properties, and module design criteria. The most significant applications of these novel membrane operations, concerning pure/fresh water production, wastewater treatment, concentration of agro food solutions, and concentration/crystallization of organic and biological solutions, are also presented and discussed.

Keywords: Membrane distillation, osmotic distillation, membrane crystallization, microporous hydrophobic membranes

INTRODUCTORY OVERVIEW ON MEMBRANE CONTACTOR SYSTEMS

Beginning from the electronic industry, the huge perspectives of the miniaturization concept are now permeating practically all manufacturing processes,

Received 31 May 2004, Accepted 29 October 2004
Address correspondence to Enrico Drioli, University of Calabria, Department of Chemical Engineering and Materials, Via P. Bucci CUBO 45/A, Arcavacata di Rende 87030, Italy. Fax: 39-0984-496692; E-mail: e.drioli@unical.it

with noteworthy repercussions on chemical engineering science and technology. Since the past decade, the philosophy of chemical processes miniaturization was known as process intensification, a design strategy aiming to lead concrete benefits in manufacturing and processing, substantially shrinking equipment size, boosting plant efficiency, saving energy, reducing capital costs, minimizing environmental impact, increasing safety, improving remote control and automation (1).

In this contest, membrane processes showed great potential to replace conventional energetically intensive techniques such as distillation and evaporation, to accomplish the selective and efficient transport of specific components, to improve the performance of reactive processes and, in ultimate instance, to provide reliable options for a sustainable industrial growth. At present, the possibility to realize compact and small-size membrane systems able to perform the same standard unit operations—the core of the chemical industry and of any other industrial processing involving molecular transformations—is becoming reliable. The redesign of important production cycles by combining various membrane operations available in the separation and conversion units represents a reliable and attractive opportunity due to the synergic effects that can be reached.

Traditional membrane separation systems, such as Reverse Osmosis (RO), Microfiltration (MF), Ultrafiltation (UF), Nanofiltration (NF), Electrodialysis (ED), Pervaporation (PV), etc., that have already gained wide acceptance in many different areas, are today completed with new membrane systems. Among them, Membrane Contactors technology probably offers the most powerful tools for inter phase mass transfer based on the principles of phase equilibria (Table 1).

Such extremely compact devices are able to immobilize gas or liquid interface at the membrane pores due to the hydrophobic nature of the membrane itself, and to create a large contact area for promoting an efficient mass transfer. Gas and liquid flowrates can be independently controlled without any physical limitation (loading, flooding, etc.). In addition, they are modular for an easy scale-up and can be efficiently integrated into new or pre-existing production lines; in general, membrane contactors are added in parallel to increase the system capacity, and in series to improve the degree of separation.

Gas/liquid membrane contactors have been tested in a large variety of systems, including absorption into aqueous or organic solutions of CO_2, SO_2, NO, H_2S, NH_3, etc., carbonation of beverages, nitrogenation of beer to provide a dense foam head, oxygen removal in semiconductor industry for the production of ultrapure water, ozonation for water treatment that represent today well-assessed commercial applications (3).

Microporous hollow fibres have been used also in dehumidification processes as absorption air-handling systems working with liquid desiccants. In this case, membrane contactors are able to achieve a considerable saving

Table 1. Advanced Membrane Contactor systems (reported in second reference)

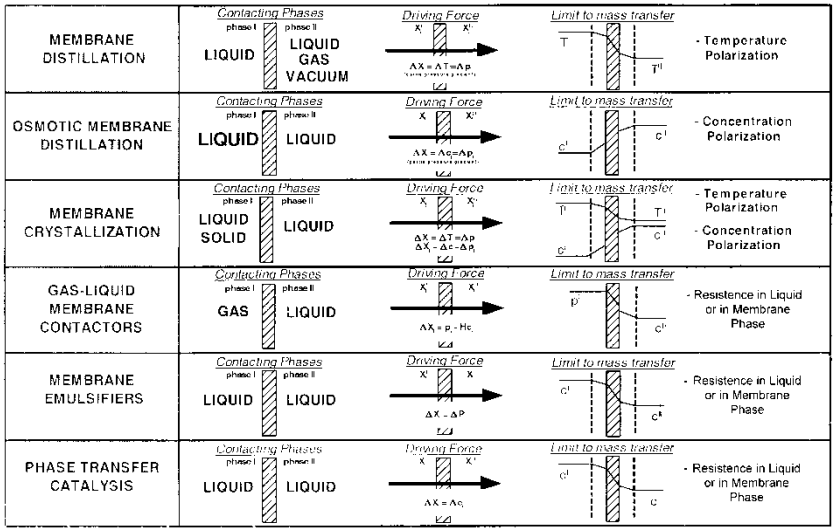

of energy by performing desiccant reactivation at moderate temperature (40–60°C) (4).

In phase transfer catalysis operations, microporous membranes assure a well-defined separation and contact between gas and liquid. At the same time, the catalytically active phase deposited on the surface of inorganic membrane layers promotes the reaction between absorbed reactant species (5). It is well recognized that the yield of ethanol and various metabolic compounds can be significantly improved if the reaction products are removed in situ by membrane contactors (6). This concept has been successful extended also to the enzymatic hydrolysis of triglycerides with simultaneous separation of the glycerol and fatty acids produced (7).

Membrane Contactor technology can be applied to produce uniform emulsions with reduced energy input and wall shear stress with respect to high-pressure homogenizers and rotor/stator systems. In a membrane emulsifier, high-stability droplets are created by forcing the dispersed phase through the nanopores of a membrane (8).

Membrane distillation (MD) and Osmotic distillation (OD) are well-known methodologies having great potential as concentration processes carried out at low temperature (9). Both operations involve microporous hydrophobic membranes that are in contact with aqueous solutions at different temperatures and/or compositions. As further requirements, the membrane should not be wetted by the process liquids, no capillary condensation should take place inside the pores of the membranes, and only vapour should be transported.

MD and OD operations are not significantly affected by concentration polarization phenomenon, whereas it represents the critical limit for pressure driving processes such as NF or RO. Production of high purity distillate, absence of limitation caused by fouling, possibility to drive MD by low enthalpy sources (solar (10), geothermal (11), etc.) that are not expected to play a significant role in other conventional operations such as Multi-Stage Flash (MSF) or Multi-Effect Distillation (MED) (12), are significant advantages for this membrane operation. In addition, MD can be conveniently integrated to conventional MED or RO processes in order to increase the recovery factor of the desalted water and/or improve the energetic efficiency of the system (13). Separations by MD and OD include cases where the product is represented by the permeate (desalination, wastewater treatment), the concentrate (foodstuffs), and both streams (azeotropic separations).

Crystallization from solution is a widely utilized unit operation due to its ability to provide large amounts of high-purity products in one processing step. The recent development of a membrane crystallization (MCr) unit, aiming to induce supersaturation in solution, has been successfully tested in the crystallization of ionic salts, low molecular organic acids, and proteins; potential applications in the desalination industry are also increasing in interest (14).

This review addresses the fundamental concepts and the relevant mathematics related to the transport phenomena through microporous hydrophobic membranes of interest in MD, OD, and MCr; membrane preparation, and material properties and module design criteria are also discussed. In the second part of the paper, some of the most promising applications and perspectives of these membrane operations are presented.

MEMBRANE DISTILLATION: OPERATIONAL PRINCIPLES

In MD process, a microporous hydrophobic membrane is in contact with an aqueous heated solution on one side (feed or retentate). The hydrophobic nature of the membrane prevents a mass transfer in liquid phase and creates a vapour-liquid interface at the pore entrance. Here, volatile compounds evaporate, diffuse and/or convect across the membrane pores, and are condensed and/or removed on the opposite side (permeate or distillate) of the system (Figure 1).

Basic MD principles can be individuated in the U.S. patent application granted to Bodell in early 1963 (15), and first experimental results on MD, published by Findley in 1967 (16). An interesting and extensive historical excursus on membrane distillation has been reported by Lawson and Lloyd (9).

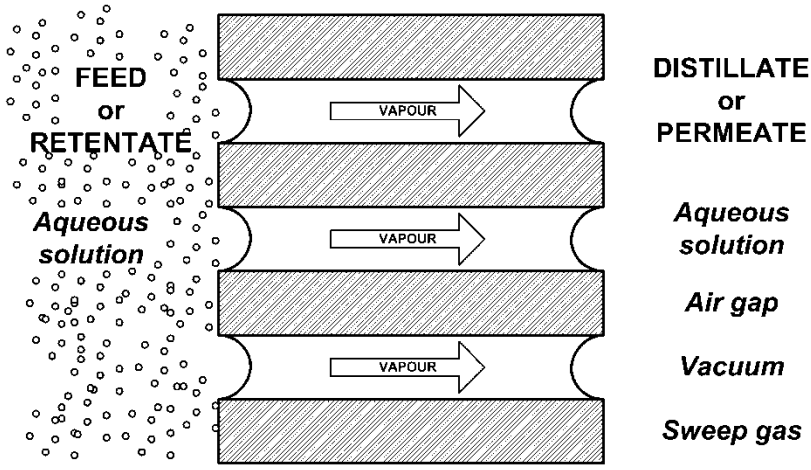

Figure 1. A general scheme of the MD process.

The specific method used to activate the vapour pressure gradient across the membrane, representing the driving force for this operation, characterizes each of the four basic MD configurations. In the most common arrangement—known as direct contact membrane distillation (DCMD)—the permeate side of the membrane consists of a condensing fluid (often pure water) that is directly in contact with the membrane. Both feed and permeate flows may be operated in counter current, relatively high heat-transfer coefficients are reachable, and horizontal or perpendicular installation of membrane modules is realizable. Alternatively, the vaporized solvent is recovered on a condensing surface that can be separated from the membrane by an air gap (AGMD), vacuum (VMD), or removed by a sweep gas (SGMD). All described configurations are schematised in Figure 2.

The nature of the driving force, in synergy with the hydro-repellent character of the membrane, allows the complete rejection of non-volatile solutes such as macromolecules, colloidal species, ions, etc. Lower temperatures and pressures with respect to those usually used in conventional distillation column are generally sufficient to establish a quite interesting transmembrane flux, with consequent reduction of energy costs and mechanical requirements of the membrane. Typical feed temperatures vary in the range of 30–60°C, thus permitting the efficient recycle of low-grade or waste heat streams, as well as the use of alternative energy sources (solar, wind, or geothermal). In addition, the possibility of using plastic equipment also reduces or avoids erosion problems. If compared to RO process, MD does not suffer limitations arising from concentration polarization phenomenon and can be

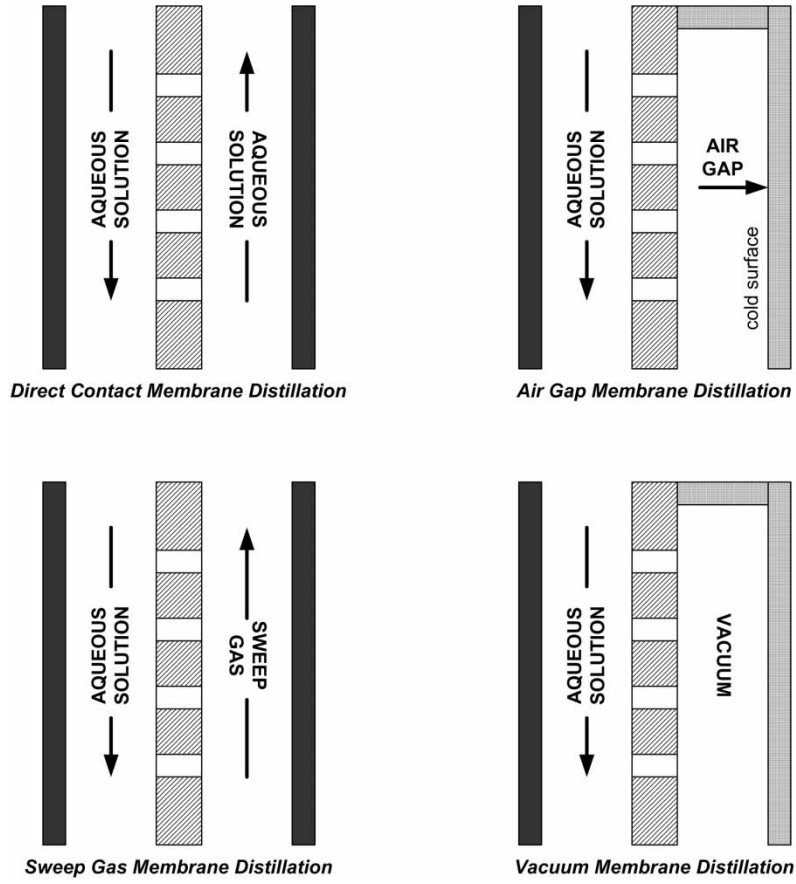

Figure 2. Schematic representation of the various MD configurations (adapted from (9)).

preferentially employed whenever elevated permeate recovery factors or high retentate concentrations are requested. Figure 3 compares both RO and MD transmembrane fluxes measured during orange juice concentration tests: while the RO flux drastically drops off due to an increase of osmotic pressure with concentration, the MD flux slightly decreases as a consequence of both reduction of the activity coefficient, and increase of the feed solution viscosity.

Driving Force and Vapour-Liquid Equilibrium

Heat and mass transport through membranes occurs only if the overall system is not in thermodynamic equilibrium. In membrane processes, two

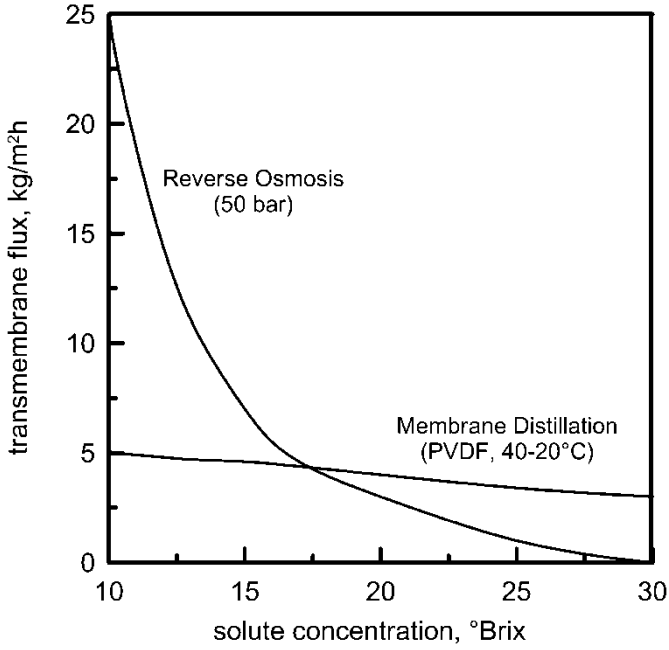

Figure 3. Comparison of RO and MD fluxes for concentrating orange juice (adapted from (17)).

homogeneous subsystems (with defined values of chemical potential μ_i' and μ_i'') are separated by a membrane.

For small changes of the number of moles in the two phases (caused by the mass transfer across the membrane), the variation of the Gibbs free energy (G) is:

$$dG = \sum_i \left(\mu_i' - \mu_i''\right) dn_i' \tag{1}$$

Relation (1) expresses a general concept: the driving force for the mass transport of a component from one phase to the other is given by the difference in the chemical potential of the two phases caused by changes in temperature, pressure and activity. In equation (1), n_i' is the mole of i-th component transferred and is related to transmembrane flux J_i by:

$$\frac{dn_i'}{dt} = AJ_i \tag{2}$$

where t indicates the time and A the membrane area.

As previously stated, the hydrostatic pressure gradient across the membrane is negligible in MD, and the driving force of process is the

partial pressure difference across the membrane, established by a temperature difference between the two contacting solution, or by vacuum, air gap, or sweep gas in the permeate side. In the frequent case of non-ideal mixtures, the vapour-liquid equilibrium is mathematically described in terms of partial pressure (p_i), vapour pressure of pure i (p_i^0), and activity coefficient ξ_i, according to the well-known thermodynamic relationship:

$$p_i = Py_i = p_i^0 a_i = p_i^0 \xi_i x_i \tag{3}$$

In equation (3), P is the total pressure, a_i the activity, and x_i and y_i are the liquid and vapour mole fraction, respectively. The vapour pressure p^0 of a pure substance varies with temperature according to the Clausius-Clapeyron equation:

$$\frac{dp^0}{dT} = \frac{p^0 \lambda}{RT^2} \tag{4}$$

where λ is the latent heat of vaporization ($\lambda = 9.7$ cal/mol for water @ 100°C (18)), R the gas constant, and T the absolute temperature.

At the pore entrance, the curvature of the vapour-liquid interface is generally assumed to have a negligible effect on the equilibrium; however, possible influences on the vapour pressure value can be estimated by the Kelvin equation:

$$p^0_{convex\ surface} = p^0 \exp\left[\frac{2\gamma_L}{rcRT}\right] \tag{5}$$

where r is the curvature radius, γ_L the liquid surface tension, and c the liquid molar density.

Activity coefficients ξ_i can be deduced by a large variety of equations aiming to evaluate the excess Gibbs function of mixtures; the most popular of them are reported in Table 2 (19). The Margules equation is the simplest one, and has been found to give similar results to the Van Laar equation for several organic solutions. For asymmetric systems showing large positive deviation from ideality, the Van Laar equation is used preferentially. The Wilson equation is a powerful tool for systems that do not exhibit liquid-liquid phase splitting. A most flexible and complex approach to the determination of activity coefficients is given by the UNIQUAC equation; it is based on a combinatorial term that contains pure-components parameters, and a residual contribution depending on adjustable parameters that are characteristic for each binary system.

NRTL model (20) is also frequently used in the description of vapour-liquid equilibrium of binary mixtures; for ethanol-water mixtures, Sarti and

Table 2. Empirical expressions for the activity *coefficients* (ξ_i^{∞} *is the activity* coefficient at infinite dilution)

Margules equation	$\frac{G^E}{RT} = (A_{21}x_1 + A_{12}x_2)x_1x_2$	
	$\ln \xi_1 = x_2^2[A_{12} + 2(A_{21} - A_{12})x_1]$	$\ln \xi_1^{\infty} = A_{12}$
	$\ln \xi_2 = x_1^2[A_{21} + 2(A_{12} - A_{21})x_2]$	$\ln \xi_2^{\infty} = A_{21}$
Van Laar equation	$\frac{G^E}{RT} = \frac{A'_{12}A'_{21}x_1x_2}{A'_{12}x_1 + A'_{21}x_2}$	$\ln \xi_1^{\infty} = A'_{12}$
	$\ln \xi_1 = \frac{A'_{12}A'_{21}x_1x_2}{(A'_{12}x_1 + A'_{21}x_2)^2}$	$\ln \xi_2^{\infty} = A'_{21}$
	$\ln \xi_2 = \frac{A'_{21}A'_{12}x_1^2}{(A'_{12}x_1 + A'_{21}x_2)^2}$	
Wilson equation	$\frac{G^E}{RT} = -x_1 \ln(x_1 + \Lambda_{12}x_2)$	$\ln \xi_1^{\infty} = -\ln \Lambda_{12} + 1 - \Lambda_{21}$
	$-x_2 \ln(x_2 + \Lambda_{21}x_1)$	
	$\ln \xi_1 = -\ln(x_1 + \Lambda_{12}x_2)$	$\ln \xi_2^{\infty} = -\ln \Lambda_{21} + 1 - \Lambda_{12}$
	$+x_2\left(\frac{\Lambda_{12}}{x_1 + \Lambda_{12}x_2} - \frac{\Lambda_{21}}{x_2 + \Lambda_{21}x_1}\right)$	
	$\ln \xi_2 = -\ln(x_2 + \Lambda_{21}x_1)$	
	$+x_1\left(\frac{\Lambda_{21}}{x_2 + \Lambda_{21}x_1} - \frac{\Lambda_{12}}{x_1 + \Lambda_{12}x_2}\right)$	

co-workers (21) reported the following expressions:

$$\ln \xi_i = x_k^2\left[\tau_{ki}\left(\frac{G_{ki}}{x_i + x_kG_{ki}}\right)^2 + \frac{\tau_{ik}G_{ik}}{(x_k + x_iG_{ik})^2}\right] \tag{6a}$$

$$\tau_{ik} = a_{ik} + \frac{b_{ik}}{T}; \quad G_{ik} = \exp(-\Omega\tau_{ik}) \tag{6b}$$

where x_i and x_k are the mole fractions of ethanol and water, respectively; constant values are $a_{ik} = 0.49854$, $b_{ik} = -456.00$, $\Omega = 0.24$.

The expression for activity coefficient in diluted aqueous ionic solutions can be derived from the Debye-Hückel theory:

$$\log \xi_{\pm} = -|z_+z_-|\Psi\sqrt{I} \tag{7a}$$

Here $\xi_{\pm}$ is the activity coefficient of the electrolyte, Ψ is a constant that depends on the temperature and solution permittivity, z is the ion valence, and

I the ionic strength of the solution given by:

$$I = \frac{1}{2}\sum_i z_i^2 c_i \tag{7b}$$

In an aqueous solution at 25°C the constant Ψ is 0.509 $(\text{mol kg}^{-1})^{1/2}$ (22).

Mass and Heat Transfer Through Microporous Hydrophobic Membranes

Mass Transfer: Model of Resistances

According to the usual electrical analogy, mass transport for a typical membrane distillation process is conveniently described in terms of serial resistances upon transfer between the bulks of two phases contacting the membrane (Figure 4). Mass transfer boundary layers adjoining the membrane generally result in a negligible contribution to the overall mass transfer resistance, whereas molecular diffusion across the polymeric membrane often represents the controlling step. Resistance to mass transfer on the distillate side is omitted whenever MD operates with pure water as condensing fluid in direct contact with the membrane, or if the configuration used to establish the required driving force is based on vacuum. The resistances within the membrane are associated to Knudsen, molecular and surface diffusion mechanisms, and convective transport.

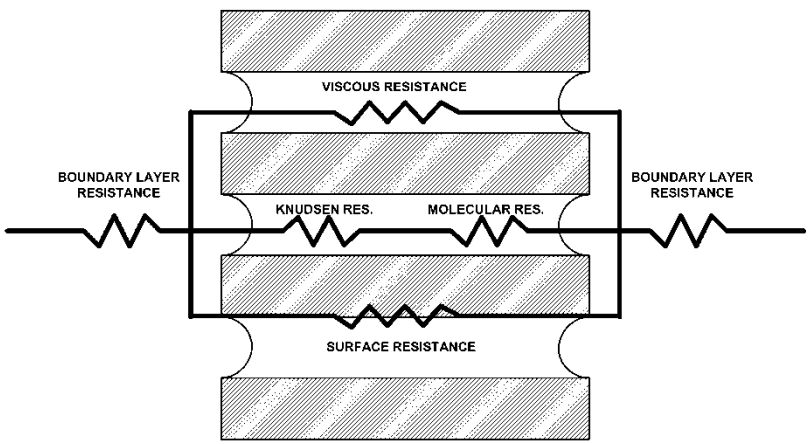

Figure 4. Serial and parallel arrangement of resistances to mass transport in MD.

Mass Transfer Boundary Layer Resistances

In a thermally driven membrane distillation process, the increase of the overall resistance to mass transfer as result of the presence of a mass transfer boundary layer in proximity of the membrane interface is generally negligible (23). On the other hand, this aspect has to be carefully evaluated if crystallization or precipitation processes can occur, because it might induce a different level of supersaturation in proximity of the membrane.

A mass balance across the feed side boundary layer allows to derive a relationship between molar flux J, the mass transfer coefficient k_x, and solute concentrations c_m and c_b at the membrane interface and in the bulk, respectively:

$$\frac{J}{\rho} = k_x \ln \frac{c_m}{c_b} \tag{8}$$

ρ is the density of the solution. Literature provides several correlations (24), often derived by analogy with those evaluated for heat transport, that are practical for determining the mass transfer coefficient. These empirical relationship are usually expressed in the form:

$$Sh = \alpha \mathrm{Re}^{\beta} Sc^{\gamma} \tag{9}$$

where:

- Sh, Sherwood number $Sh = (k_x\, d_h)/D$ (d_h: hydraulic diameter, D: diffusion coefficient)
- Re, Reynolds number $\mathrm{Re} = (\rho\, v\, d_h)/\mu$ (ρ: fluid density, v: fluid velocity, μ: fluid viscosity)
- Sc, Schmidt number $Sc = \mu/(\rho\, D)$

A brief list of mass transfer correlations for Newtonian fluids is given in Table 3.

As consequence of the solvent permeation through the membrane, solute concentration c_m at the feed solution/membrane interface becomes higher than that in the bulk solution, c_b. This phenomenon, known as concentration polarization, is quantified by the CPC coefficient, defined as:

$$CPC = \frac{c_m}{c_b} \tag{10}$$

Mass Transfer: Transport Across the Membrane

In a porous medium, if surface diffusion is assumed negligible (33), mass transfer can be affected by viscous resistance (resulting from the momentum transferred to the supported membrane), Knudsen diffusion resistance (due to

Table 3. Predicative equations for mass transfer coefficients

	Comments	Reference
Equation (tube side flow)		
$Sh = 0.023Re^{0.8}Sc^{0.33}$	Chilton-Colburn, $Re > 10^5$, $Sc > 0.5$	(25)
$Sh = 0.34Re^{0.75}Sc^{0.33}$	Chilton-Colburn, $10^4 < Re < 10^5$, $Sc > 0.5$	(25)
$Sh = \frac{(f/2)ReSc}{1 + 5\sqrt{f/2}(Sc - 1)}$	Prandtl–Taylor	(25)
$Sh = \frac{(f/2)ReSc}{1 + 5\sqrt{f/2}[Sc - 1 + \ln(1 - 5Sc)/6]}$	Von-Karman	(25)
$Sh = 0.023Re^{0.875}Sc^{0.25}$	$300 < Sc < 700$	(26)
$Sh = 0.0149Re^{0.88}Sc^{0.33}$	$Sc \geq 100$	(27)
$Sh = 0.023Re^{0.83}Sc^{0.44}$	$0.6 < Sc < 2.5$	(28)
Equation (shell side flow)		
$Sh = 1.25\ (Re\ d_e/L)^{0.93}Sc^{0.33}$	$0.5 < Re < 500$, $\phi = 0.03$	(29)
$Sh = 0.019\,Gz$	$Gz = \frac{\dot{m}}{\rho DL}$ ($\dot{m}$: mass flow rate) $Gz < 60$, close-packed fibers	(30)
$Sh = 1.38\ Re^{0.34}Sc^{0.33}$	$1 < Re < 25$, $\phi = 0.70$	(29)
$Sh = 0.90\ Re^{0.40}Sc^{0.33}$	$1 < Re < 25$, $\phi = 0.07$	(29)
$Sh = 0.46\ Re^{0.46}Sc^{0.33}$	Baffled cylindrical module	(31)
$Sh = 0.57\ Re^{0.31}Sc^{0.33}$	Liquid flow perpendicular to the fibers	(32)

collisions between molecules and membrane walls) or ordinary diffusion (due to collisions between diffusing) molecules (34). Predominance, coexistence, or transition between all of these different mechanisms are estimated by comparing the mean free path ι of diffusing molecules to the mean pore size of the membrane (Knudsen number). Kinetic theory of ideal gases calculates ι as:

$$\iota = \frac{k_B T}{P\sqrt{2}\pi\sigma^2} \tag{11}$$

where k_B is the Boltzmann constant ($1.380 \cdot 10^{-23}\,JK^{-1}$), and σ is the collision diameter of the molecule ($\sigma = 2.7$Å for water).

For the binary mixture of water vapour in air, the free mean path $\iota_{a/w}$ can be evaluated at the average membrane temperature $\bar{T}$, by (35):

$$\iota_{a/w} = \frac{k_B \bar{T}}{\pi((\sigma_w + \sigma_a)/2)^2 P} \frac{1}{\sqrt{1 + (m_w/m_a)}} \tag{12}$$

where σ_a (=3.7 Å) and σ_w are the collision diameters, and m_a and m_w the molecular weight for air and water, respectively. For an average temperature $\bar{T} = 60^{\circ}C$, Phattaranawik and colleagues (36) reported a mean free path of 0.11 μm.

In the continuum region, the free mean path of a gas is small if compared with the average membrane pore diameter, and molecule-molecule collisions predominate over molecule-wall collisions. Knudsen number, defined as the ratio of the free path of the gas to the pore diameter ($Kn = \iota/d_{pore}$) is <1 and the flux can be described by Darcy's law. In the Knudsen region this situation is reversed: the mean free path of a gas is large with respect to the average membrane pore diameter ($Kn > 1$), molecule-wall collisions predominate over molecule-molecule collisions and the mass transport can be described by Knudsen's law. In many practical cases, ι is comparable to the typical pore size of MD membranes and no simplifications can be done when modelling MD mass transfer operations. Dusty Gas Model (DMG) is frequently used for describing gaseous molar fluxes through porous media; the most general form (neglecting surface diffusion) is expressed as (37):

$$\frac{J_i^D}{D_{ie}^k} + \sum_{j=1\neq i}^{n} \frac{y_j J_i^D - y_i J_j^D}{D_{ije}^0} = -\frac{1}{RT}\nabla p_i \tag{13a}$$

$$J_i^v = -\frac{\varepsilon r^2 p_i}{8RT\tau\mu}\nabla P \tag{13b}$$

$$D_{ie}^k = \frac{2\varepsilon r}{3\tau}\sqrt{\frac{8RT}{\pi M_i}} \tag{13c}$$

$$D_{ije}^0 = \frac{\varepsilon}{\tau} D_{ij}^0 \tag{13d}$$

where J^D is the diffusive flux, J^v the viscous flux, D^k the Knudsen diffusion coefficient, D^0 the ordinary diffusion coefficient, y the molar fraction in gaseous phase, p the partial pressure, M_i the molecular weight, μ the gas viscosity, r the pore radius, ε the membrane porosity, and τ the membrane tortuosity. Underscript *e* indicates the "effective" diffusion coefficient, calculated by taking into account the structural parameters of the membrane as shown in equations (13c) and (13d).

Although DGM was derived for an isothermal systems, it is successfully applied in MD working under relatively small thermal gradients by assuming an average value of temperature across the membrane. Studies looking at de-aerating the feed solutions demonstrated the possibility to achieve flux improvements as result of a decrement of the molecular diffusion resistances, which makes Knudsen flow dominant (38, 39).

Simplifications related to particular MD configurations are summarised in Table 4. Despite the modest complexity of the proposed fundamental models, the adoption of empirical correlations is in some cases preferred.

Table 4. Simplified equations for the mass transfer through microporous membranes

Configuration	Assumption	Transport equation
Vacuum membrane distillation (limited by Knudsen diffusion)	Mean pore size $\ll \iota$	$J_i = \frac{D_{ie}^k}{RT}\nabla p_i = \frac{2\varepsilon r}{3\tau RT}\sqrt{\frac{8RT}{\pi M_i}}\nabla p_i$ (40)
Air gap membrane distillation (limited by diffusion through stagnant air)	Air is considered as stagnant film $\gamma = 2.334$ if water is the sole diffusion specie (41)	$J_i = D_{i-air,e}^0 \frac{T^{(\gamma-1)/\gamma}}{R\lvert p_{air}\rvert_{ln}}\nabla p_i$ (42)
Air filled pores direct contact membrane distillation (Knudsen-molecular diffusion transition)	Mean pore size $\approx \iota$	$J_i = -\frac{1}{RT}\left[\frac{1}{D_{ie}^k} + \frac{p_{air}}{D_{ije}^0}\right]^{-1}\nabla p_i$ (9)
De-aerated direct contact membrane distillation (Knudsen-Viscous transition)	Knudsen diffusion resistance dominant. Existence of viscous flux	$J_i = -\frac{1}{RT}\left[\frac{2\varepsilon r}{8\tau}\sqrt{\frac{8RT}{\pi M_i}}\nabla p_i + \frac{\varepsilon r^2}{8\tau}\frac{p_i}{\mu}\nabla P\right]$ (9)

The transmembrane flux is often expressed as a linear function of the vapour pressure difference across the membrane (43):

$$J = C\Delta p \tag{14}$$

where C is the membrane distillation coefficient, and Δp the partial pressure gradient evaluated at the membrane surfaces. In equation (14), the membrane distillation coefficient C is a function of the structural membrane properties (pore size, thickness, porosity, and tortuosity), physical and chemical properties of the vapour transported across the membrane (molecular weight and diffusivity), and operative conditions (44–46).

Heat Transfer: Model of Resistances

Complex relations between simultaneous heat and mass transfer are generally described in terms of a set of serial and parallel resistances through the boundary layers of the membrane and through the membrane itself. Figure 5 illustrates this situation in the case of DCMD; simplifications deriving from the possibility to omit one or more resistances can be made for specific MD configurations.

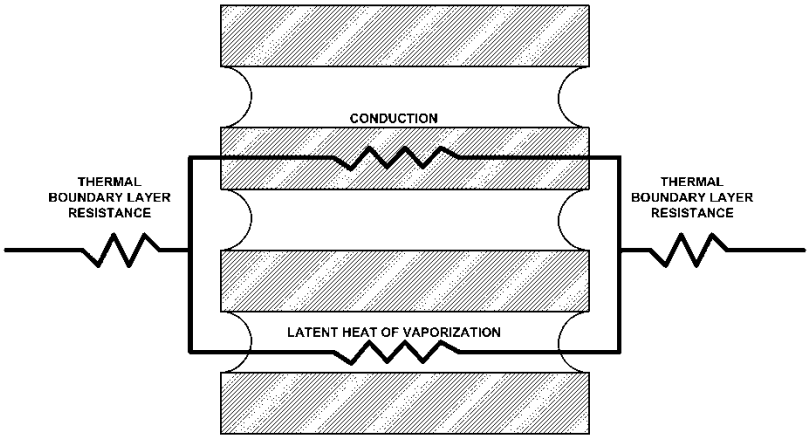

Figure 5. Serial and parallel arrangement of resistances to heat transfer in MD.

Boundary-layer heat transfer is recognized as the limiting factor of the transport efficiency, and several efforts (use of spacers, turbulence promoters or turbulent flow) aim to minimize the external resistances. The heat transport across the membrane mainly occurs according to two different mechanisms: conduction across the polymeric material, and latent heat flow related to vaporized components. The total heat flux Q transferred across the membrane is expressed as (9):

$$Q = \left[\frac{1}{h_f} + \frac{1}{h_m + N_i\lambda/\Delta T_m} + \frac{1}{h_p}\right]^{-1} \Delta T \tag{15}$$

where λ is the molar heat of vaporization, ΔT_m is the temperature difference across the membrane, ΔT is the bulk temperature difference between retentate and permeate, h_f, h_m, and h_p are the heat transfer coefficients on the feed side, membrane, and permeate side, respectively.

Heat Transfer Boundary Layer Resistances

The most detrimental effect of the thermal boundary layer resistances is that the temperature in the bulk differs from the value at membrane-solution interface where vapour-liquid transition occurs. Temperature polarization coefficient is generally used to quantify the magnitude of the boundary layer resistances over the total heat transfer resistance. It is defined as:

$$TPC = \frac{T_f^m - T_p^m}{T_f - T_p} \tag{16}$$

TPC, often used as indirect index of efficiency for MD process, falls between 0.4 and 0.7 for a satisfying design of the system, and approaches

unity for mass transfer limited operations. Literature data provide a large variety of empirical correlations that allow to evaluate the boundary layer heat transfer coefficient *h.* Apart from the previously defined Reynolds' number, most of these correlations involve some additional dimensionless numbers:

- Nu, Nusselt number $Nu = (hD)/k$ (k: thermal conductivity)
- Gr, Grashof number $Gr = (D^3\rho^2 g\beta\Delta T)/\mu^2$ (g: gravity acceleration, β: thermal expansion coefficient)
- Pr, Prandtl number $\mathrm{P}r = (c_p\mu)/k$ (c_p: specific heat)
- Gz, Graetz number $Gz = (\dot{m}c_p)/kL$ ($\dot{m}$: mass flow rate, L: fiber length)

A brief summary of useful empirical relationships is proposed in Table 5.

High feed flowrates through hollow fiber modules, resulting in increased Reynolds number, improve the heat transport efficiency of MD operations (52). Spacers can have benefits in MD, since they destabilize the flow and create eddy currents in the laminar regime enhancing momentum, heat, and mass transfer (53, 54).

Table 5. Predictive equations for heat transfer coefficients

Equation	Comments	Reference
$Nu = 0.13\ \mathrm{Re}^{0.64}\ \mathrm{Pr}^{0.38}$	Laminar flow	(47)
$Nu = 0.097\ \mathrm{Re}^{0.73}\ \mathrm{Pr}^{0.13}$	Laminar flow	(47)
$Nu = 1.62(\mathrm{Re}\ \mathrm{Pr}(d/L))^{0.33}$	Laminar flow	(42)
$Nu = 0.023\mathrm{Re}^{0.8}\mathrm{Pr}^{0.33}\left(\mu/\mu_w\right)^{0.14}$	Turbulent liquid	(48)
$Nu = 3.66 + \dfrac{0.067Gz}{1 + 0.04Gz^{0.66}}$	Laminar flow, VMD	(21)
$Nu = 0.036\mathrm{Re}^{0.8}\mathrm{Pr}^{0.33}(d/L)^{0.055}$	Turbulent flow	(49)
$Nu = 0.027(1 + (6d/L))\mathrm{Re}^{0.8}\mathrm{Pr}^{0.33}\left(\mu/\mu_w\right)^{0.14}$	Turbulent flow	(49)
$Nu = 1.75\ \{Gz + 0.04[(d/L)\ Gr\ \mathrm{Pr}]^{0.75}\}^{0.33}$	Important influence of free convection	(50)
$Nu = 0.116(\mathrm{Re}^{0.66} - 125)\mathrm{Pr}^{0.33} \times [1 + (d/L)^{0.66}]\left(\mu/\mu_w\right)^{0.14}$	Transition region	(51)

An heat transfer correlation for DCMD with spacers was obtained from the mass transfer correlation for UF assuming analogy between heat and mass transfer (55):

$$Nu = k_{dc} 0.664 \,\mathrm{Re}^{0.5} \mathrm{Pr}^{0.33} \left(\frac{2d_{h,s}}{l_m}\right)^{0.5} \tag{17.a}$$

with

$$k_{dc} = 1.654 \left(\frac{d_f}{H}\right)^{-0.039} \varphi^{0.75} \left[\sin\left(\frac{\phi}{2}\right)\right]^{0.086} \tag{17.b}$$

Here, k_{dc} is the correction factor for spacer geometry, $d_{\mathrm{h,s}}$ the hydraulic diameter for the spacer-filled channel, d_{f} filament size, l_{m} the mesh size, H the spacer thickness, φ the spacer voidage, and ϕ the hydrodynamic angle. Figure 6 better clarifies the meaning of these parameters.

Heat Transfer: Transport Across The Membrane

The total heat flux Q is transferred across the membrane by two mechanisms: conduction across the membrane material, and as latent heat associated to the vaporized solvent. The differential balance of energy is expressed as:

$$Q = JH_v(T) - k_m \frac{dT}{dx} \tag{18}$$

where $\mathrm{H_v}$ is the (vapour) enthalpy at temperature T, $\mathrm{k_m}$ is the thermal conductivity of the membrane, and x the distance. Assuming $\mathrm{T_0}$ as a reference temperature, and considering that temperature inside membrane changes within

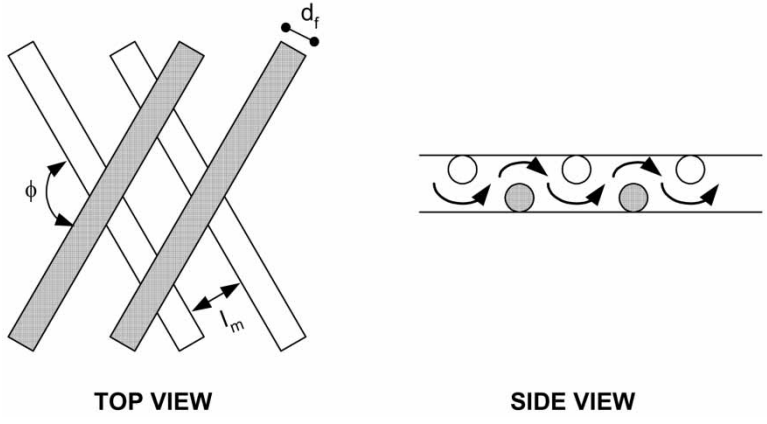

Figure 6. Flow direction in spacer-filled channel (adapted from (55)).

few degrees—so that the specific heat can be supposed constant—the vapour enthalpy at a generic temperature T is given by:

$$H_v(T) = \lambda(T_0) + c_{pv}(T - T_0) \tag{19}$$

Here c_{pv} is the specific heat of vapour. Whereas the latent heat of vaporization is effectively used to promote the permeate flux, the conduction of heat across the membrane is an energetic loss that need to be minimized. According to the investigation of Fane and co-workers (38), the heat loss by conduction represents the 20–50% of the overall heat transferred in MD.

In order to study the evaporation efficiency in MD, Martiez-Diez and collegues (56) have carried out experiments on PTFE microporous membranes and aqueous NaCl solutions. In the range of investigated parameters, the heat lost by conduction per unit transmembrane flux was found to decrease with increasing temperatures and flow rates. The efficiency of MD can be also increased from 8% to 14% by reducing the permeate temperature (57). The conduction heat transfer coefficient k_m for a two-phase composite material is generally calculated by the Isostrain model (58):

$$k_m = (1 - \varepsilon)k_s + \varepsilon k_g \tag{20}$$

assuming that both polymer (k_s) and gas (k_g) contribute to k_m.

The values of membrane thermal conductivity found by equation (20) agree with measured ones within 10% (39). The thermal conductivity of polymers strongly depends upon temperature and degree of crystallinity. Lost by conduction is reduced by increasing membrane porosity, since the water vapour thermal conductivity is one order of magnitude lower than that of polymeric materials in the range of typical MD working temperatures (59).

Heat transferred by convection is generally considered negligible with exception of AGMD process (60).

Models and Numerical Procedures

Several numerical studies and approaches with different levels of complexity have been addressed to the modelling of MD process; some of them are briefly mentioned next. In the work of Laganà et al. (23), momentum, mass, and heat balance equations have been written in cylindrical coordinates for a steady-state 3-D flow through microporous hollow fibers, assuming axial diffusion negligible, no radial dependence of the pressure, Newtonian fluid behaviour; authors reported a good agreement between simulated results and experimental data.

Bouguecha and colleagues (52), used the stream function-vorticity approach and assumed constant properties except for the density in the

body force term; the coupled elliptic transport equations for momentum, heat, and mass have been written in Cartesian coordinates for steady-state 2-D laminar natural convection.

An analytical solution for a longitudinal segment model to be used as sub-model for more sophisticated configurations of shell-side packing in tubular-type unit has been presented by Agashichev and Falalejev (61). The solution, that does not contain differential terms and permits estimation of heat flux and temperatures at the membrane interface, is applicable to laminar, incompressible and continuous flow through a triangular membrane bundle packed uniformly.

The analytical estimation of temperatures at the membrane interface has been derived by Gryta and co-workers (50) for DCMD process in a plate-and-frame module with laminar flow, and successfully extended to MD capillary modules. The simplified differential (mono-dimensional) balance was solved for steady-state condition, assuming that the amount of heat transferred to and from the surface adjacent to the membrane is equal to the amount of heat transferred inside the membrane.

A simple iterative procedure to solve simultaneously mass and energy (mono-dimensional) balances has been reported by Fane et al. (38). A Monte Carlo simulation model has been recently developed by Imdakm and Matsuura (62) to study vapour permeation through membrane pores in DCMD. A three-dimensional network of interconnected cylindrical pores with a pore size distribution represented the porous membrane. The model took into account all molecular transport mechanisms based on the kinetic gas theory. Model prediction was in good qualitative agreement with available experimental data.

Osmotic Membrane Distillation

Osmotic membrane distillation (OD) is a concentration technique for aqueous mixtures in which water is removed from the feed by a hypertonic solution flowing downstream a microporous hydrophobic membrane. Water vapour diffuses through the membrane pores under a driving force given by the vapour pressure difference between both membrane sides, related to the water activities in the two streams.

OD is not a purely mass transfer operation: water transport implies evaporation at the feed side and condensation at the extract side. A temperature difference at the membrane interfaces is thus created, even if the bulk temperatures of the two liquids are equal. Mengual et al. (63) estimated the temperature difference in their aqueous system to be lower than 1°C, which would lead to a negligible decrease of the vapour flux. Following a simplified approach, the transmembrane flux can be expressed in terms of membrane permeability K_m, vapour pressures p_w^I at feed (1) and stripping (2)

fluid-membrane interfaces, and log mean pressure of air entrapped into pores $\bar{p}_{air}$:

$$J = K_m \frac{p^I_{w1} - p^I_{w2}}{\bar{p}_{air}} \tag{21}$$

Water vapour pressure is related to activity by equation (3). Referring to a series expansion cut at the first-order term, and assuming that the temperature difference through the membrane is small, the following relationship can be derived (64):

$$J = \frac{K_m}{\bar{p}_{air}} \left\{ p^0_w(\bar{T}) \cdot \left[a^I_{w1} - a^I_{w2}\right] - a_w(\bar{T}) \cdot \left[\frac{dp_w}{dT}\right]_{\bar{T}} \left(T^I_2 - T^I_1\right) \right\} \tag{22}$$

where p^0 is the vapour pressure of pure liquid, a_w is the water activity, and $\bar{T}$ is the average temperature between the two membrane interfaces.

Film-theory model can be used to describe the mass transport through boundary layers:

$$J = k_x \rho \ln \frac{x^I}{x} \approx k_x \rho \frac{a_w - a^I_w}{\xi_w \bar{x}} \tag{23}$$

assuming that water activity coefficient ξ_w is constant in the layer; k_x is the mass transfer coefficient, x the solute mole fraction and $\bar{x}$ its logarithmic mean value. Temperature and activity gradients can act in a synergistic way, or can operate in an antagonistic way to each other. Heat transfer phenomena are described as in MD operations. The salts chosen as osmotic pressure agents are in general NaCl (because of its low cost), $MgCl_2$, $CaCl_2$, and $MgSO_4$ (65). In osmotic evaporation carried out at room temperature, transmembrane fluxes generally range between 0.2 and $0.4\,L/m^2h$ (66).

Membrane Crystallization

Membrane Crystallization (MCr) has been recently proposed as one of the most interesting and promising extension of the MD concept (14). This innovative technology uses the evaporative mass transfer of volatile solvents through microporous hydrophobic membranes in order to concentrate feed solutions above their saturation limit, thus attaining a supersaturated environment where crystals may nucleate and grow.

Crystallization is today a routinely used unit operation both for purification and separation steps, but the design and operation of a crystallizer still pose many problems. Industrial equipments often produce crystals that do not satisfy the specific quality criteria, that are becoming more and more stringent due to the shift of the market trend from base chemicals towards

life-science products. The opportunity to couple membrane processes and crystallization operations has been reported in the scientific literature since the past decade. Slurry precipitation and recycle reverse osmosis (SPARRO) technology (67) for desalting scaling mine waters (where uncontrolled $CaSO_4$ precipitation is a crucial problem at relatively high ionic concentrations) is a significant example of such integration. Sluys and colleagues (68) illustrated the concept of a membrane-assisted crystallizer in the softening of drinking water by removing $CaCO_3$. According to their operation scheme, the suspension of seeds covered with crystallized material, leaving a crystallizer unit, is treated in a pressure driven membrane filtration stage; here, the membrane concentrates the suspension to the mass percentage required for seeding.

As previously discussed, mass transport through microporous hydrophobic membranes has an advantage over pressure driven membrane systems as concentration process at high solute concentrations. In fact, the reduction of vapour pressure caused by high concentration and viscosity is modest if compared to RO process, where elevated hydrostatic pressures are required to overcome the osmotic phenomena occurring in concentrate streams.

With respect to conventional crystallizers, the laminar flow of the solution through tubular or capillary membranes improves the homogeneity of the mother liquor, reduces mechanical stress, and promotes an oriented organization of the crystallizing molecules. As a consequence, crystals exhibiting good structural properties and narrow size distribution are generally produced in membrane crystallization devices.

Crystal size distribution (CSD) is a critical parameter for precipitation and crystallization processes. Relatively large crystals limit the adhesion of mother liquor after filtration and, therefore, show a low tendency toward caking. On the contrary, small crystals are preferentially requested whenever reduced dissolution times are needed. In all cases, narrow distributions are necessary.

The mass distribution $W(L_i)$ can be expressed in term of the mass fraction of crystals belonging to a certain size class divided by the width of the size class (ΔL_i) (69):

$$W(L_i) = \alpha \rho_c L_i^3 \frac{\Delta N_i}{\Delta L_i} \tag{24}$$

α is the volume shape factor, ρ_c is the crystal density, ΔN the number of crystals—counted in a unit volume of slurry—having length between L and $L + \Delta L$.

Apart from the average sizes evaluated by distribution diagrams, the width of a distribution around the mean size is often characterized by the coefficient of variation (CV), equal to the standard deviation divided by

the mean size (69):

$$CV = \left\{ \left[\frac{\int_0^\infty (L - L_{50\%})^2 W(L) dL}{\int_0^\infty W(L) dL} \right]^{1/2} \right\} \cdot \frac{\int_0^\infty W(L) dL}{\int_0^\infty L W(L) dL} \tag{25}$$

$L_{50\%}$ is the crystal length corresponding to a value of $W(L)$ equal to 50%. A narrow CSD is characterized by a low CV. Experimental CV values measured in membrane crystallization tests carried out on NaCl range within 15–30% (14); as term of comparison, a CV of about 50% is obtained when using a conventional mixed-suspension crystallizers (70).

The role of a membrane is not only limited to furnish a support for solvent evaporation. A crystallizing solution can be imagined as a certain number of solute molecules moving among the molecules of solvent and colliding with each other, so that some of them converge forming clusters, or growth units. In general, these clusters have a larger probability of being dissolved than of continuing to grow but, under specific conditions, critical nuclei having the same probability of growth as of dissolution can be generated. All those clusters with a size larger than the size of the critical nucleus (r^*) will be likely to grow spontaneously. There is, therefore, an energetic barrier ΔG^* (the nucleation barrier) that must be crossed in order to induce the formation of stable nuclei (71):

$$\Delta G^* = \frac{16 \pi \nu^2 \gamma^3}{3[kT \ln S]^2} \tag{26}$$

where ν is the molar volume occupied by a growth unit, γ the surface energy, and S the supersaturation.

The values of r^* and ΔG^* vary inversely with supersaturation: r^* tends to infinity as S tends to 1. The existence of this energy barrier explains why a solution that should experience homogeneous precipitation under thermodynamic conditions does so only if a certain value of supersaturation is exceeded.

The presence of a polymeric membrane in the crystallizing solution decreases the work required to create critical nuclei and increases locally the probability of nucleation with respect to other locations in the system: this phenomenon is known as heterogeneous nucleation. Considering the interaction between solute and substrate in terms of contact angle θ that the crystallizing solution forms with the substrate, the reduction of the activation energy (71) is given by following equation

$$\Delta G^{het} = \Delta G^{\text{hom}} \left[\frac{1}{2} - \frac{3}{4} \cos \vartheta + \frac{1}{4} \cos^3 \vartheta \right] \tag{27}$$

If the solution wets the substrate completely ($\theta = 180^\circ$), $\Delta G_{het} = \Delta G_{hom}$; when the contact angle is 90° (limit between hydrophobic and hydrophilic

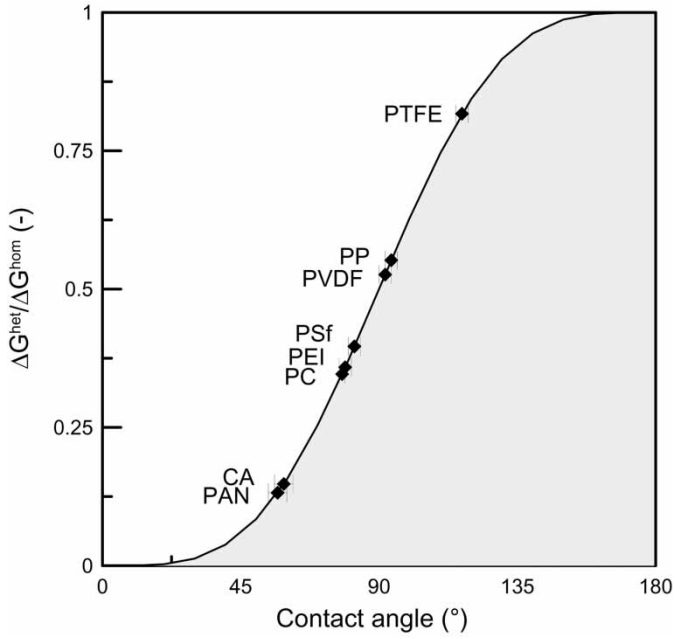

Figure 7. Reduction in the free energy of the nucleation barrier due to heterogeneous nucleation as a function of the water contact angle with the polymeric surface (CA: cellulose acetate; PAN: polyacrylonitrile; PC: polycarbonate; PET: polyetherimide; PES: polyethersulfone; PP: polypropylene; PSf: polysulfone; PTFE: polytetrafluoroethylene; PVDF: polyvinylidenefluoride).

behaviour), $\Delta G_{het} = 1/2\Delta G_{hom}$. This concept, exemplified in Figure 7 for the familiar case of water in contact with several polymeric membranes (but extendable by analogy to any kind of solution), might represent the starting point for a better engineering of the crystallization procedures. Experimental results show that the nucleation rate B in a membrane crystallizer depends on the concentration of crystals in the magma (m_T), hydrodynamics (e.g., stirrer speed, pump impeller, rotation rate: Φ), and difference Δc between the mother liquor concentration and the value at equilibrium (solubility) (69):

$$B = k_b m_T^i \Phi^j \Delta c^k \tag{28}$$

Typical values of k_b lie between 1 and 2.5; i is close to 1 whenever collisions between crystals and vessel walls dominate on crystal-crystal interactions. The overall growth rate G is usually related to the overall concentration driving force Δc by an empirical relation (69):

$$G = k_G \Delta c^g \tag{29}$$

where g is the overall order of the growth process, and k_g is the growth rate constant that is function of temperature, controlling kinetic mechanism (diffusion or integration), presence of impurity in the system. Further details about crystal nucleation and growth kinetics can be found in the specific literature (70–72).

MATERIALS

Preparation and Modification of MD Membranes

In MD, membrane is not involved in the transport phenomena on the basis of its selective properties. Volatile compounds are transferred across the membrane according to vapour-liquid equilibrium principia, whereas the microporous polymeric material acts as physical barrier between two phases and sustains the interfaces where heat and matter are simultaneously exchanged. Since the hydrophobic character of the membrane represents a crucial requirement, membranes have to made by polymers with a low value of surface energy. Polymers such as polypropylene (PP), polytetrafluoroethylene (PTFE), and polyvinylidenefluoride (PVDF) are commonly employed in the preparation of membranes for MD applications (73). PP in isotactic configuration (surface energy: $30.0 \times 10^{-3}\,\mathrm{N/m}$) exhibits excellent solvent resistant properties and high crystallinity. PTFE membranes (surface energy: $9.1 \times 10^{-3}\,\mathrm{N/m}$) are highly crystalline and show excellent thermal stability and chemical resistance (they are low soluble in practically all common solvents). PVDF membranes (surface energy: $30.3 \times 10^{-3}\,\mathrm{N/m}$) exhibit good thermal and chemical resistance. This polymer is soluble in aprotic solvents such as dimethylformamide (DMF), dimethylacetamide (DMAc), and triethylphosphate (TEP).

Microporous hydrophobic membranes are manufactured by sintering, stretching, and phase inversion (73–75): for instance, PP membranes are generally prepared by stretching and thermal phase inversion, PTFE membranes by sintering or stretching, PVDF membranes by phase inversion.

Sintering is a simple technique: a powder of polymeric particles is pressed into a film or plate and sintered just below the melting point. The process yields to a microporous structure having a porosity in the range of 10–40% and a rather irregular pore size distribution. The typical pore size, determined by the particle size of sintered powder, typically ranges from 0.2 to 20 μm.

Microporous membranes can be also prepared by stretching an homogeneous polymer film made from a partially crystalline material. Films are obtained by extrusion from a polymeric powder at temperature close to the melting point coupled with a rapid draw-down. Crystallites in the polymers are aligned in the direction of drawing; after annealing and cooling, a mechanical stress is applied perpendicularly to direction of drawing. This

manufacturing process gives a relatively uniform porous structure with pore size distribution in the range of 0.2–20 μm and porosity of about 90%.

A large part of commercially available membranes are prepared by phase inversion process (76) by dissolving the polymer in an appropriate solvent and spreading it, as a 20–200 μm thick film, on proper supports. The homogeneous solution splits in two phases by adding an appropriate precipitant (typically water): a solid polymer rich phase and a liquid rich phase are formed.

The precipitated polymer exhibits a quite uniform porous structure: a large variety of pore sizes (from 0.2 to 20 μm) can be obtained by varying the polymer concentration, the precipitation medium, temperature, etc. Almost all soluble polymers can be precipitated in a non-solvent. Since PP is not readily dissolved at room temperature, a solution of 20–30% polymer is spread at elevated temperature into a film. Precipitation does not occur by addition of non-solved, but by cooling the solution to a de-mixing point. Extraction of the solvent is typically done by low molecular weight alcohols.

Details about commercial membranes used in studies of MD are given in (77). Recently, some significant results reached in the preparation and modification of polymeric membranes have provided to an increase of the reliability of MD process. Copolymers of tetrafluoroethylene (TFE) and 2,2,4-trifluoro-5-trifluoromethoxy-1,3-dioxole (TTD), commercially known as HYFLON AD, have been used for preparing asymmetric and composite membranes that show a high contact angle (~120°) for water, demonstrating a highly hydrophobic character (78).

PVDF asymmetric hollow fiber membranes have been prepared by introducing small molecular additives in dimethylacetamide (DMAC) as nonsolvents (water, ethanol, i-propanol) and LiCl salt. The wet prepared fibers exhibited high water permeability and the dry fibers had high gas permeability, good mechanical strength, and excellent hydrophobicity (79). Asymmetric hydrophobic microporous membranes from the copolymer of PTFE and PVDF have been recently obtained by phase inversion process (80). According to the experimental analysis, these membranes exhibit excellent mechanical properties (stretching strain and extension ratio at break approximately 6–8 times higher PVDF) and high hydrophobicity (contact angle to water of 88.5°).

The recent work of Xu and colleagues (81) showed that hydrophobic PTFE membranes with a protective hydrophilic sodium alginate coating were resistant to wet-out at least for 300 minutes during OD tests using feeds containing 0.2, 0.4, and 0.8 wt.% orange oil. The reduction in the overall mass transfer coefficient due to the coating was less than 5%.

Low pressure plasma techniques are non-thermodynamic-equilibrium processes that allow a change in chemical composition and properties of a material, such as wettability, dyeability, refractive index, hardness, etc. A very high hydrophobicity, somewhat higher than that of PTFE, was

achieved by fluorinated coatings also named "Teflon-like" (82). Kong and coworkers (83) have modified hydrophilic microporous cellulose nitrate membranes by plasma polymerization of octafluorocyclobutane. The performance of these membranes, tested in MD applications, was found comparable with that of usual hydrophobic polymers.

Polyetherimide (PEI) flat sheet membranes were modified by Khayet and colleagues (84) using fluorinated surface modifying macromolecule. Membranes were prepared by phase inversion method from casting solutions containing the solvent NJ-dimethylacetamide and the non-solvent y-butyrolactone. Contact angle measurements showed that the PEI membrane surface became more hydrophobic after modification, while X-ray photoelectron spectroscopy analysis showed enrichment of fluorine on the PEI membrane surfaces.

Hydrophobic Properties, Contact Angle and Surface Tension Measurements

Information about hydrophobicity is obtained by contact angle (θ) measurements (85, 86): a droplet of water deposited on a hydrophobic surface gives a contact angle greater than 90°. According to the Young equation:

$$\gamma_{LV} \cos\theta = \gamma_{SV} - \gamma_{SL} \tag{30}$$

where γ_{LV}, γ_{SV}, and γ_{SL} are the surface tension for liquid-vapour, the surface energy of the polymer, and the solid-liquid surface tension, respectively. Because surface tensions involving a solid cannot be measured directly, a second equation is required. Using a thermodynamic approaches, Newmann (87) established the following equation of state:

$$\gamma_{SL} = \gamma_{SV} + \gamma_{LV} - 2\sqrt{\gamma_{SV}\gamma_{LV}} \exp\left[-\beta\left(\gamma_{SV} - \gamma_{LV}\right)^2\right] \tag{31}$$

and, combining it with the Young equation:

$$\cos\theta = -1 + 2\sqrt{\gamma_{SV}/\gamma_{LV}} \exp\left[-\beta\left(\gamma_{SV} - \gamma_{LV}\right)^2\right] \tag{32}$$

where β is a parameter independent of the solid and liquid used.

When using the highly complex Good, van Oss, and Chaudhury method (88), three reference liquids (typically water, di-iodomethane, and glycerol) are used to determine the apolar γ_{LW}, acid base γ_{AB}, acid (electron acceptor) γ^+, base (electron donor) γ^- components of the surface energy. For instance, di-iodometane (apolar test liquid) allows the evaluation of the

Lifshitz-van der Waals component γ_s^{LW} of the membrane surface tension:

$$\gamma_s^{LW} = \frac{\gamma_l^{LW}(1-\cos\theta)^2}{4} \tag{33}$$

Subscripts s and l indicate solid (membrane) and liquid, respectively.

Other components are calculated by the following equations:

$$\gamma_{LV}(1+\cos\theta) = 2\left(\sqrt{\gamma_s^{LW}\gamma_l^{LW}} + \sqrt{\gamma_s^+\gamma_l^-} + \sqrt{\gamma_s^-\gamma_l^+}\right) \tag{34a}$$

$$\gamma_{AB} = 2\sqrt{\gamma_s^-\gamma_s^+} \tag{34b}$$

Typical contact angle of water ($\gamma_{LV} = 72.2\,\mathrm{mN/m}$) are close to 120° on PP (89), are of about 108° and 107° on PTFE and PVDF, respectively (90).

The applicability of exposed relationships is practically limited, because they have been derived for ideal surfaces (smooth and homogeneous, rigid, chemically inert).

The effect of surface heterogeneity on contact angle is generally established by relation (35) that allows to predict the contact angle θ^* of a rough surface from the contact angle θ of the equivalent smooth surface (91):

$$\cos\theta^* = f_1\cos\theta - f_2 \tag{35}$$

where f_1 and f_2 are the fractions of liquid-solid and liquid-air surfaces, respectively.

For MD membranes with surface porosity lower than 0.5, it is generally assumed that $f_1 = y, f_2 = 1-y$ and $1-y = \varepsilon/\tau$, where ε is the porosity and the pore tortuosity τ. For PTFE membranes, M. Courel and colleagues (92) have developed a more specific model:

$$\cos\theta^* = y^2\cos\theta - (1-y)^2 - 2y(1-y)\sqrt{\frac{\gamma_{SV}}{\gamma_{LV}} - \cos\theta} \tag{36}$$

From comparing experimental results and theoretical calculations, Franken and colleagues (91) concluded that contact angle measurements on homogeneous smooth materials are not suitable for an accurate description of the membrane wetting phenomenon in MD. Wettability criteria based on the concept of penetration surface tension (defined as the surface tension of the liquid on the verge of penetrating a porous medium, and measured by penetrating drop method) provided more satisfying results.

Breakthrough Pressure and Membrane Wettability

In MD operations, the penetration of liquid through the micropores of a polymeric membrane should be avoided. In general, non-wetting fluid does not pass through pores as long as the pressure is kept below a critical threshold known as breakthrough pressure. The Laplace equation offers a relationship between the pore size of the membrane r_{pore} and the breakthrough pressure ΔP:

$$\Delta P = -\frac{2\Theta\gamma\cos\theta}{r} \tag{37}$$

Here γ is the interfacial tension, Θ is a geometric factor related to the pore structure (equal to 1 for cylindrical pores), and θ the liquid-solid contact angle. This angle increases with increasing polarity difference between polymeric membrane and liquid. Breakthrough pressure data for several membranes type and fluid can be found in literature (93); in the most part of considered cases, ΔP values range between 100 and 500 kPa.

Breakthrough pressure is drastically reduced in presence, even at trace level, of detergents and surfactants (because their reduce the surface tension), or solvents that exhibit the same behaviour. Experimental investigations (94) demonstrated that, once a membrane is wetted by the penetrating liquid, a decreasing in hydrostatic pressure is not able to restore the original un-wetted condition. For mixtures of water and ethanol, Gostoli and Sarti (95) observed that the liquid entry pressure decreased linearly with alcohol concentration until the membrane was freely wetted at ethanol concentration of 75 wt%.

Effect of Membrane Pore Size Distribution

An inadequate knowledge of the morphology of a microporous membranes can lead to inaccuracy when modelling the mass transfer (96). A good agreement between theoretical and experimental results has been obtained by Martinez-Diez and Vazquez-Gonzalez (97) using pore sizes measured by mercury porometry and liquid displacement methods.

The attention to the structural properties of microporous polymeric membranes involved in MD operations is today increasing significantly.

If $f(r')$ is the normalized distribution, and $J(r')$ the transmembrane flux through all pores with radii equal to r', the total flow rate $J_T(r)$ through the membrane is obtained by the following integral relation:

$$J_T = \int_0^\infty J(r')\pi(r')^2 f(r')dr' \tag{38}$$

For instance, a lognormal distribution of pores appears in the form:

$$f(r) = -\frac{1}{SD_{\log} r\sqrt{2\pi}} \exp\left\{-\frac{1}{2}\left[\frac{\ln(r/\bar{r})}{SD_{\log}}\right]^2\right\} \tag{39}$$

where $f(r)$ is the number of pores with pore radius r, $\bar{r}$ the mean pore radius, and SD_{log} the standard deviation of lognormal function.

Laganà and co-workers (23) studied the effect of shape of pore size distribution with Gaussian (symmetric) and logarithmic (asymmetric) distribution functions; in this investigation, non-symmetrical distribution achieved better agreement with the experimental results. Several mathematical models aiming to examine the influence of both pore size distribution and air flux in DCMD were presented by Phattaranawik et al. (36). In particular, the log-normal distribution was used to represent the shape of pore size distribution. In conclusion of their work, authors reported that the predictions of the fluxes and MD coefficients showed good agreement with the experimental results for GVHP-PVDF(Millipore, 0.22 μm) and excellent agreement for HVHP-PVDF (Millipore, 0.45 μm) and PTFE (Sartorius, 0.2 μm). Additionally, the models predicted fluxes with less than 8% discrepancy.

The investigation carried out by Martinez and colleagues (98) on three commercial membranes frequently used in MD applications showed that the MD water vapour transfer coefficients, calculated considering the pore size distributions, are similar to the ones obtained assuming an average pore size model, and the permeabilities calculated from air-liquid displacement measurements agree well with those obtained in literature MD models.

Membrane Fouling

The phenomenon of flux decay in MD has been often observed in long-term operation [99, 100]. The most accredited explanation considers that trans-membrane flux falls down as consequence of fouling. Membrane biofouling due to growth of micro-organisms present in raw water often causes pore clogging, as well as an increase in pressure drop along the module. Chemical disinfection associated to UV treatment has been proposed to control biofouling; however, bacteria embedded on a polymeric surface show a significant resistance to biocides. In a recent study, Gryta (101) observed that membranes used for the treatment of saline wastewater by MD were significantly biofolued by *S. faecalis* bacteria and *Aspergillus* fungi; in addition, PP membranes appeared unable to reject *S. faecalis* bacteria, which were detected on the membrane surface on the distillate side. The presence of fungi in the membrane pores was observed only on the feed side. Flux is also reduced by scaling, occurring whenever the concentration of dissolved salts and minerals overcomes the solubility limit. Solid

precipitation on membrane surface can lead to both pore clogging and pore wetting.

The presence of particulate and colloids in the processed liquid can also induce fouling, being these particles preferentially trapped at the membrane-liquid interface by interfacial tension forces (42). In these cases, a pre-filtering of the feed solution is generally sufficient to limit the flux decay effect (102). Membrane fouling is a severe problem particularly in foods concentration; again, a preliminary ultrafiltration treatment for heavy fouling feeds can be useful in order to remove larger particles that could increases the viscosity of the stream through MD or OD units (103).

Cleaning Procedures

Cleaning procedures for hydrophobic membranes impose specific problems, particularly in processes involving fats and proteins that can adhere and foul the membrane, or alcohols and surfactants that can cause leakage. Open literature suggests few approaches to this difficult task. Efficient cleaning methods were assessed for tomato paste fouled OD membranes by Durham and Nguyen (104). The most effective cleaner for membranes with a surface tension greater than 23 mN/m was 1% NaOH; the hydrophobic integrity of these membranes was destroyed during repeated fouling/cleaning trials. The most effective cleaner for membranes with a surface tension less than 23 mN/m was P3 Ultrasil 56; water vapour flux was maintained and there was not salt leakage during repeated fouling/cleaning runs.

A steadily decreasing of transmembrane flux due to wetting phenomena was observed after 30 hours by Udriot and colleagues (105) during MD tests aiming to increase the ethanol production in a fermentation bath. In this case, the membrane was regenerated by washing with 1 M NaOH followed by ethanol aqueous solution (85% v/v) and drying with air.

DESIGN CONFIGURATIONS

MD Membrane Modules

A large variety of membrane configurations, including flat sheet (plate-and-frame and spiral wound modules), tubular (tubular, capillary, and hollow fibre modules) have been tested in MD applications. The most part of laboratory scale modules are designed for use with flat sheet membranes due to their versatility and simplicity of the preparation process; from an industrial standpoint, hollow fibre modules are more attractive due to their high specific surface area. The choice of a module is usually determined by both economic and operative conditions. An important criteria is based on an efficient control of concentration polarization and membrane fouling. In an

increasing number of cases, module are today designed and commercially available for specific applications and, in principle, they provide the best technical solution.

In plate-and-frame modules, the membranes, the porous support plates and the spacers are stacked between two endplates and placed in an appropriate housing. In this configuration, the packing density is about $100-400\,m^2/m^3$, depending on the number of membrane used. Various cassettes stacked together, each consisting of injection moulded plastic frames containing two membranes, intermediate feed channel for warm salt-water and condensing walls, have been used by Andersson et al. (106) for desalination purposes.

In spiral wound module, the feed flow channel spacer, the membrane and the porous support are enveloped and rolled around a perforated central collection tube. The feed solution moves in axial direction through the feed channel across the membrane surface. The permeate flows radially toward the central pipe. The packing density of this setup is about $300-1000\,m^2/m^3$, depending on the channel height. The use of spiral-wound MD modules at industrial level has been proposed by Gore (107) for desalination units. A spiral-wound MD module assembled by spiral winding of PTFE membrane and condenser foils has been used by Koschikowski and colleagues (108) for desalination experiments; it has been reported a specific thermal energy consumption of 140–200 kWh/m^3 of distillate (feed temperature: 60–85°C) and a gained output ratio (GOR) ranging within 4 and 6.

A tubular membrane module consists of membrane tubes placed into porous stainless steel of fiber glass reinforced plastic pipes. The diameter of tubular membranes typically vary between 1.0 and 2.5 cm, with a packing density of about $300\,m^2/m^3$. In MD operations, such kinds of modules are used for high viscous fluid; they also allow to achieve high feed flow rates that reduce fouling tendency and polarization phenomena. In a capillary membrane module, a large number of membrane capillaries (inner diameter of 0.2–3 mm) are arranged in parallel as a bundle in a shell tube; packing density is in the order of $600-1200\,m^2/m^3$.

Hollow fibre modules are based on the same concept, but differ in the dimensions of the tubular membranes. In this case, the outer diameter typically ranges between 50 and 100 μm, and several thousands of fibres are installed in the vessel. This configuration has the highest packing density ($\sim 3{,}000\,m^2/m^3$). A qualitative comparison between different membrane modules is reported in Table 6. The basic features of thermal MD modules have been listed by Schneider and co-workers (109): housing and membranes must be resistant to temperature and chemicals, capillaries have to be adequately potted free of cracks and with a good adhesion, it should be possible to dry modules accidentally wetted or repair defective capillaries, it must be ensured an uniform flow through capillaries avoiding dead corners or channel formation. Twisted or braided capillaries are able

Table 6. Comparison between different typologies of MD membrane modules

	Tabular	Plate-and-frame	Spiral-wound	Capillary	Hollow fiber
Packing density	Low	→	→	→	Very high
Investment	High	→	→	→	Low
Fouling tendency	Low	→	→	→	Very high
Cleaning	Good	→	→	→	Poor
Operating cost	High	→	→	→	Low
Membrane replacement	Yes	No	No	No	No

to fulfil the last-mentioned requirement when the parallel bundles of a large number of capillaries are difficult to realize. In general, the recommended flow velocity inside and outside the capillaries should exceed 0.1 m/s in order to achieve constantly high fluxes.

Liqui-Cel Extra-Flow technology offered by CELGARD LLC is one of the most well-known hollow fiber module for mass transfer technology (Figure 8). This module consists of thousands of microporous polypropylene fibres, with typical inside diameter and wall thickness of 240 and 30 μm, respectively. A central shell side baffle improves efficiency by minimizing by-passing and provides a component of fluid velocity normal to the membrane surface, thus improving the mass transfer rate. Liqui-Cell modules vary from 2.5 inches in diameter (1.4 m^2 membrane area) to 10 inches in diameter (130 m^2 membrane area).

Microdyn Technologies offers several MD capillary modules with tubular membranes made in PP. The inside diameter of the capillaries varies from 0.6 mm to 5.5 mm, while the number of capillaries ranges between 40 and 80. The DISSO$_3$LVE module, made in expanded PTFE membrane fibres, is marketed by W. L. Gore & Associates. Fibres (diameter: 1.7 mm, wall thickness: 0.5 mm) are arranged in helix geometry, thus offering higher mass transfer coefficients with respect to conventional parallel configuration of fibres. In general, well designed membrane modules should provide high mass and heat transfer rates, and reduce concentration polarization and fouling phenomena.

Process Enhancement

In the past few years, additional innovations in module design and new strategies have been explored in order to limit the concentration polarization phenomena and to enhance the mass transfer. Some of these techniques,

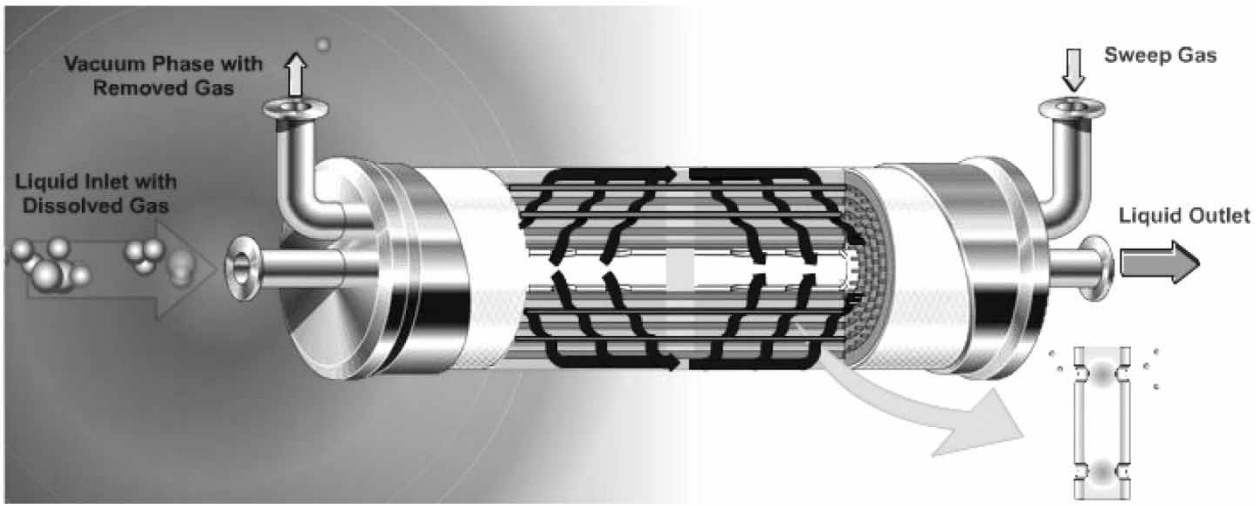

Figure 8. Scheme of the membrane contactor Liqui-Cel (CELGARD LLC) ⟨www.liquicel.com⟩.

although specifically developed for pressure-driven membrane operations, are of interest also for MD systems. The most direct approaches to polarization reduction are the hydrodynamic methods that generate flow instabilities.

Any technique that interrupts the formation of a continuous boundary layer on the transfer surface, and that promotes mixing of the fluid across the flow channel, is likely to reduce polarisation phenomena and to enhance transmembrane flux. Different alternative geometries that offer higher mass transfer coefficients than conventional parallel flow have been examined recently. In the "Kenics" mixer, helically twisted tapes are fitted closely inside tubes to promote helical fluid flow; after every half turn the direction of the helix is changed from right-handed to left-handed, thereby regularly disrupting the flow (110).

The formation of Dean vortices mixes the bulk with the wall layers and reduce polarisation without moving the membrane or the module or having flow reversal in the feed stream via inserts or otherwise. Although Dean flows satisfy the exigencies of an efficient membrane process, such as high mass transfer rate by increased wall shearing, radial mixing, and low polarisation, the presently employed modules still have the problem of low packing density and increased pressure drop (111).

Concentration and temperature polarization are reduced by the presence of turbulence promoters, also called spacers, which enhances the mass flux by increasing the film heat transfer coefficient. The spacer changes the flow characteristics and promotes regions of turbulence so improving boundary layer transfer (53).

Ultrasonic enhancement, mainly induced by ultrasonic cavitations, acoustic streaming, and ultrasonic heating, has been also applied successfully to membrane distillation processes in order to increase the system performance; some experimental results demonstrated the possibility to improve the trans-membrane flux up to 200% with an ultrasonic intensity from 0 to $5\,W/cm^2$ (112).

Lawson et al. (113), looking at the effect of membrane compaction on the membrane permeability, concluded that the transmembrane flux in MD can be increased significantly (up to 11%) with relatively small pressure drops ($<70\,kPa$).

APPLICATIONS

In spite of their potentialities and advantages with respect to conventional operations, membrane distillation and osmotic distillation technologies did not satisfy the initial expectations: MD and OD are currently used mostly at the laboratory scale. However, some pilot plant applications have recently come up, and various fields of interest are currently envisaged at laboratory stage.

Potential applications related to membrane crystallization process are still under evaluation at lab scale, but the interest aroused as consequence of a preliminary dissemination activity in international conferences and workshops on industrial crystallization encourage further investigations.

The applications of thermal and osmotic membrane contactors are frequently limited to treatment of aqueous solutions. From a practical point, four sections have been identified: pure/fresh water production, waste-water treatment, concentration of agro food solutions, concentration/crystallization of organic and biological solutions. In absence of explicit statement, the selected applications presented in the following paragraphs refer to literature studies at laboratory level.

Pure/Fresh Water Production

The production of high-purity water, fully demineralised, or drinking water from the sea represents today the main MD application. This is due to the fact that, in principle, the process rejection for non-volatile dissolved compounds is 100%.

Since 1982, Gore proposed the use of two different MD membrane modules for desalting NaCl aqueous solutions: a flat membrane for AGMD (production rate: $7\,L/m^2h$, $T_{feed} = 30^\circ C$, $T_{distillate} = 20^\circ C$), and a spiral-wound module (production rate: $3\,L/m^2h$, $T_{feed} = 30^\circ C$, $T_{distillate} = 20^\circ C$) (107).

A few years later, literature papers related to the use of MD in desalination processes were increased exponentially (106, 114, 115, 116).

DCMD carried out by PTFE microporous membranes was considered by Godino et al. (117) for obtaining pure water from NaCl brines. Their work investigated the influence of temperature, fluid-dynamics, and salt concentration of the system efficiency. According to the obtained results, transmembrane flux increased of about 100% when the retentate temperature was shifted from 30 to 50°C, while flux decreased of about 20% when feed concentration increased from 0.5 to 2.0 mol/L. Banat and Simandl (118) used an AGMD module for carrying out desalination experiments on PVDF membrane sheets. Very pure water with less than 5 ppm TDS was obtained in all experiments, whose reproducibility was $\pm 20\%$.

The combined use of DCMD and solar energy was investigated by Morrison et al. (119) by developing a simulation model of membrane distillation combined with TRNSYS solar simulation system. This study demonstrated the economic feasibility of the solar powered plant if a 60–80% is recovered. More recently, the sensitivity of the permeate flux to the brine temperature, flow rate, salt concentration and solar irradiation has been evaluated by Banat and colleagues (120). Fresh water was simultaneously produced by the solar iron still and the membrane module, but the contribution of solar still was no more than 20% of the total flux.

The experimental analysis of Lawson and Lloyd (121) indicated that DCMD is a viable process for seawater desalination, with fluxes reaching up to 2.0 mol/m^2s working at feed temperature of 75°C and distillate temperature of 20°C; these fluxes are two times higher than practical RO ones. In addition, concentration measurements carried out on the permeate stream revealed a quasi-total rejection of NaCl molecules.

Schneider et al. (109) stated that thermal membrane distillation was not able to compete with large-scale multi-effect evaporators for seawater desalination. Small and portable desalination units utilising waste heat, that are simple in design and afford easy access, have been identified as market niches that MD may fill.

First assessments of the process economics gave indications that the use of PTFE membranes for desalting seawater raises the costs of MD to an excessively high level (114) mainly due to the elevated price of the commercial membrane modules; however, this trend is now reversing. Papers addressed to seawater desalination by membrane distillation have continued to proliferate also in more recent years (122–125).

The most interesting perspectives for the development of membrane distillation/crystallization technology probably are related to the possibility to combine them with other conventional pressure driven membrane processes. The possibility to integrate RO and MD for increasing the water recovery factor in desalination plants has been proposed by Drioli and co-workers (126). By coupling these two membrane units, a global recovery factor of 87.6% was obtained; the reduction of discharged brine is also expected to reduce the environmental impact. If a membrane crystallizer takes the place of the MD unit, rejected brines can be further concentrated in order to promote the nucleation and growth of sodium chloride crystals (127).

A detailed energetic and exergetic analysis, carried out on an integrated NF/RO/MD system (128), showed that 13 kWh/m^3 are required to drive the plant, but this value falls down to 2.6 kWh/m^3 if low grade thermal energy is available. In this case, the total operating costs are of 0.56 $\$/m^3$. The combined use of a gas-liquid membrane contactor, a conventional precipitator and a membrane crystallizer was successfully applied to nanofiltration retentate for the recovery of salts dissolved in seawater (129). Calcium carbonate was removed up to 89%; 35.5 kg of NaCl and 8.4 kg $MgSO_4 \cdot 7H_2O$ per cubic meter of NF retentate were obtained. In addition, the amount of water condensed in the distillate side at the membrane crystallizer allowed to increase the NF recovery factor from 64% to 95%.

Wastewater Treatment

The possibility to remove heavy metals from waste-water has been discussed by Zolotarev and colleagues (130). In particular, a rejection coefficient close

to unity was obtained by treating aqueous solutions of nickel sulphate in the range of 0.1–3.0 N. MD has been applied for the recovery of HCl from acidic spent solutions generated by cleaning of electroplated surfaces. Experiments, carried out at inlet feed and distillate temperatures of 343 K and 293 K, respectively, evidenced the possibility to attain a distillate concentration of about 100 g HCl/dm^3 with a volumetric permeate flux decreasing from 80 to 40 dm^3/m^2d (131).

MD process has been used to concentrate sulphuric acid obtained after apatite phosphogypsum extraction used to recover lanthane compounds. The concentration process was protracted up to 40% of H_2SO_4; lanthane compounds were precipitated by cooling (132).

MD has been investigated as treatment method for radioactive liquid wastes, generated from the nuclear industry, or by other end-user of radioactive materials (hospitals, nuclear R&D centres, etc.). The decontamination process-aiming to eliminate radioisotopes and to reduce the waste volume—is conventionally achieved by chemical precipitation, ion exchange and evaporation. Whereas performance of traditional pressure-driven membrane processes is limited by fouling, concentration polarization phenomena and blockage, MD run carried out under moderate conditions of temperature and pressure significantly reduces these disadvantages. In addition, this enables the use of plastics with consequent elimination of corrosion problems and reduction of installation costs. High volume reduction and decontamination factors ($\sim$4300 for ^{60}C, $\sim$44 for ^{137}Cs, $\rightarrow \infty$ for other investigated compounds) have been reached, as well as significant rejection values towards nuclides such as tritium or some forms of iodine and ruthenium (133).

Zakrzewska-Trznadel and colleagues (134) also observed the existence of a diffusion isotope effect in MD that enhances the separation factor for H_2O/DHO and $H_2^{16}O/H_2^{18}O$ enrichment. MD was successfully applied also to textile waste water contaminated with dyes (57). The dependence of distillate fluxes, rejection, and polarization phenomena on the retentate concentration, operation temperatures and axial flowrates suggested the opportunity of integrate MD operation in a production cycle with RO pre-concentration stage. Gryta et al. (135) proposed a combination of UF and MD to treat oily wastewater. Results showed that the permeate obtained from the UF process generally contains less than 5 ppm of oil. Further purification of the UF permeate by membrane distillation results in a complete removal of oil from wastewater and a very high reduction of the total organic carbon (99.5%) and total dissolved solids (99.9%)

MD operating under vacuum is an effective method for removing volatile organic components from dilute aqueous solutions (21, 40, 136) such as acetone and isopropanol, ethanol, methylterbutylether, ethylacetate, methylacetate, and benzene traces from contaminated water. The ability of microporous hydrophobic membranes to strip chloroform, tetrachloroethylene, carbon tetrachloride, 1,1,2-trichloroethane, and trichloroethylene from

aqueous solutions has been also verified (137). A characteristic of VMD is that the resistances to mass and heat transfer in the liquid phase adjacent to the membrane are often the rate limiting step in the kinetics of the separation. Urtiaga et al. (138) observed that only at higher Reynolds numbers within the turbulent flow regime the resistance to mass transfer due to vapour diffusion through the porous membrane affects the overall mass transfer coefficient.

Concentration of Agro-Food Solutions

MD works at relatively low feed temperature: this enables its application of the process to the food industry, where solutions are sensitive to high temperatures. With respect to standard concentration methods (generally a multistage vacuum evaporation) that involve a significant energy consumption and degradation of the organoleptic properties of juices, membrane distillation process represents a competitive alternative, able to increase the quality of concentrates.

DCMD was successfully tested in the concentration of many juices: orange juice (17), apple juice (23), sugarcane juice (139), etc. The technical feasibility to concentrate the must by VMD was considered by Bandini and Sarti (140), with the objective of increasing the alcoholic potential, while preserving quality and quantity of the aromas. In all cases, concentration degrees obtained (50–60°Brix) are significantly higher than those achieved by pressure driven membrane processes, such as RO. On the other hand, in the range of 10–20°Brix, the MD fluxes at 25–30°C were of the order of $1-3\,L/m^2h$, much lower than those measured for RO working at the same temperature ($10-15\,L/m^2h$). A loss in taste and flavours of the concentrate juice was also observed, due to the evaporative nature of MD process.

Due to the nature of the driving force, OD can proceed at ambient temperature, which is more attractive than MD itself. For what concerns the preparation of the striping solution, although a number of salts are suitable ($CaCl_2$, $MgCl_2$, etc.), potassium salts of ortho- and pyrophosphoric acid have gained in interest due to their safe use in foods (141, 142). Flavour and fragrance compounds can be conveniently preserved in OD concentration process, mainly because of the low temperature used; in addition, they have high molecular weights and, consequently, a low diffusive permeability through the membrane.

The integration of UF, RO, and OD units has been tested in fruit juice concentration in order to obtain high recovery factors. The investigations carried out in Melbourne (Australia) during the last few years have shown the potentiality of the membrane system for the production of grape juice concentrate and de-alcoholized wine ferments; an optimised pilot plant has been also developed for the treatment of viscous concentrates. The plant processes 50 L/h of juice that is concentrated up to 65-70°Brix. 200 mL of 70°Brix

concentrate is typically obtained from 1L of raw juice (143). The Mildura plant in Australia is operated by Vineland Concentrates and CELGARD LLC. The plant contains 22 Liqui-Cel modules (total membrane area: 425 m^2) operated at 30–35°C and 2 atm. A good retention to flavour and aroma is achieved, but module cleaning appears difficult.

More recently, the use of integrated membrane processes for the clarification and concentration of citrus (orange and lemon) and carrot juices has been proposed. A limpid phase has been produced by ultrafiltration, carried out on a pilot unit used to clarify the raw juice. The permeate coming from the UF stage has been concentrated up to 15–20 g TSS/100 g by reverse osmosis, performed on a laboratory-scale unit. Finally, osmotic distillation step yielded a concentration of the retentate coming from the RO up to 60–63 g TSS/100 g at an average transmembrane flux of about 1 kg/m^2h. A little decrease of the Total Antioxidant Activity (TAA) has been observed during the RO treatment, probably due to the mechanical stress induced by the high operative pressure. Further analysis have shown that the subsequent treatment by OD did not induce any significant change to TAA independently on the final concentration achieved (144).

Concentration/Crystallization of Organic and Biological Solutions

MD has been applied in the concentration of organic and biological solutions for selective extraction of volatile solutes and solvents. Blood and plasma were treated by MD in order to promote a solute-free extraction of water from biomedical solutions without loss in quality [145, 146]. Membrane distillation has been also suggested as innovative tool to ameliorate treatment of uraemia by allowing purification of the blood ultrafiltrate and the re-injection of the purified water to the patients. The optimisation of the overall process in terms of energetic requirements, membrane area, and operating conditions has was made by Capuano and colleagues (147) in order to propose a clinical application of the technique.

MD is also used to recovery volatile compounds such as ethanol. Alcohol is produced by fermentation of biomass in batch fermenters. The excess of ethanol in a fermentation broth inhibits the process, leading to zero the rate of bioconversion. The integration of MD downstream the fermentor improves the process: due to the difference of volatility between water and ethanol, alcohol can be removed also using a non selective microporous membrane (148–150). Gryta and co-workers (151) observed that, in the case of fermentation combined with MD, an efficiency of 0.4–0.51 (g EtOH)/(g of sugar) and a production rate of 2.5–4 (g EtOH)/dm^3 h was achieved in relation to 0.35–0.45 (g EtOH)/(g of sugar) and 0.8–2 (g EtOH)/dm^3 h obtained in the classical batch fermentation. The ethanol flux measured in MD varied in the range of

1–4 (kg EtOH)/m^2 per day and was dependent on the temperature and the feed composition.

Air-gap membrane distillation was tested by Banat and Simandl (152) for ethanol–water separation using PVDF membranes. The upper feed concentration tested was 10 wt.% ethanol. Within the feed temperature range of 40–70°C, ethanol selectivity of 2–3.5 was achieved. Of potential interest is the separation of azeotropic mixtures by AGMD suggested by Udriot et al. (105). Experiments in a plate-and-frame MD module, with azeotropic mixtures of HCl/H_2O and of propionic acid/H_2O yielded retention selectivities of the solute between 0.6 and 0.8. For the HCl/H_2O system, the apparent azeotropic point in MD was shifted to higher acid strength, whereas it disappeared for the propionic acid/H_2O system. This phenomenon was explained by the differences in the diffusion rates across the membrane and the air gap of the different components of the azeotropic mixtures.

The possibility to couple a membrane crystallization stage with a biocatalytic membrane reactor for processing in food and pharmaceutical industry has been recently verified by Curcio and colleagues (153). With respect to conventional chemical catalysts, the enzymatic catalytic act is extremely specific and efficient, thus leading to higher reaction rates in milder operative conditions. A drawback of the enzymatic reactions is represented by equilibrium constants that are generally unfavourable for total conversion to desired products. Specifically, a membrane crystallizer was employed in order to recover the unreacted fumaric acid present in the outlet stream of a membrane bioreactor in the synthesis of L-malic acid. The experimental work aimed to investigate the evolution of crystal size distribution, nucleation and growth rates as function of time, kinetic effects due to slurry density and supersaturation.

Membrane crystallization represents a promising technology that could offer an important contribution also in life science. Structural proteomic, concerning with the systematic three-dimensional structure resolution of proteins, is today a reliable approach to the comprensive understanding of biomolecular functions at atomic level. Automation and standardization of protocols, high-throughput purification strategies and advances in diffraction crystallography make production of protein crystals as the rate limiting step of the structural analysis. Although protein crystallization process shares—in principle—many common properties with that of small solutes, the structural complexity of macromolecules is a serious obstacle to their ordinate arrangement in a 3D lattice. The absence of correlation between protein properties and multiparametric sets to be screened, coupled with the extremely high failure probability recorded in crystallization trials, call for developing new ideas and innovative methods. Hen egg white lysozyme has been selected as protein model for membrane crystallization tests.

HEWL tetragonal crystals were grown on poly-propylene membranes under the following conditions: 20 mg/mL of protein in 0.1 M NaAc pH 4.6, 2–5% w/v NaCl, 20°C. Diffraction data collected at the X-ray beam line XRD-1 of the Italian synchrotron light laboratory ELETTRA (Trieste, Italy) demonstrated the excellent quality of the analysed crystals: in the best case, a diffraction high resolution limit of 1.91 Å, a mosaicity value of 0.167° and an overall mean temperature factor (<B>) of 20.4 $Å^2$ have been detected for the refined crystal structure. Overall, quality indicators are comparable with those measured for lysozyme crystals grown under micro-gravity environment (control: PDB accession code 1BWJ). Under mentioned crystallization conditions, transmembrane fluxes were in the range of 0.2–0.25 $\mu L/mm^2h$.

Short induction times, estimated by on-line turbidimetric measurements of the crystallizing solution, have been observed even at low supersaturation. When working at supersaturation ratio of 1.3–3.9, evidence of first stable nuclei after elapsed periods of 1.4–2.0 hours confirmed the significant role of heterogeneous nucleation promoted by the polymeric membrane. A comparison with kinetic data reported in literature also demonstrated that a membrane-based crystallization unit is able to speed up significantly crystal growth rate, and HEWL crystals achieved a size suitable for diffraction analysis within 16–24 hours (154, 155).

CONCLUDING REMARKS

Membrane contactors technology—and MD, OD, and MCr in particular—can potentially lead to significant innovation in processes and products, thus offering new opportunities in the design, rationalisation, and optimisation of innovative productions. Authors of this paper are strongly convinced that some of the most interesting developments are actually related to the possibility of integrating novel membrane devices together with well-assessed traditional membrane units, with overall important benefits related to a synergic interaction between them.

Despite their great potential, membrane distillation and osmotic distillation are still far to fulfil all the expectations. To overcome the existing barriers, more systematic analysis of possible advantages or drawbacks related to the introduction of an innovative membrane unit, clear protocols and comparison indexes for the choice of the best materials and operative conditions, accurate modelling for an easy scale-up or scale-down, and significant multidisciplinary research efforts are needed.

In this view, the problem of developing microporous membranes with high hydrophobic character and stability, with a narrow distribution of pore size and improved structural and morphological characteristics, is a crucial

aspect to be addressed in research programs devoted to the preparation of new specific membranes for MD and related operations. In addition, all feasible approaches devoted to increase the efficiency of these membrane contactor devices by reducing both concentration and temperature polarization phenomena, to enhance mass and heat transfer coefficients, to control the fouling problems and related drawbacks (clogging, loss of hydrophobicity etc.) are expected to be matter of further investigations for researchers working on this area.

Future applications for MD and related processes can be already anticipated in different areas and, specifically: in traditional water desalination of sea- and brackish-water, in direct competition with RO in the case of small units or when alternative energy sources are available; as integrated units for improving recovery factors of water-treatment processes; in a large variety of applications (agrofood, pharmaceutical, or biotechnological industry) where solutions showing a reduced chemical and physical stability are involved. In general—in the opinion of the authors—the fact that this kind of membrane operations well satisfy the overall strategy of Process Intensification is *per se* a sufficiently strong driving force to the use of these innovative devices as alternative to the traditional unit operations not satisfying at all the requested design criteria. However, recent developments make realistic to affirm that new wide perspectives in membrane technology and integrated membrane solutions for a sustainable industrial growth are possible.

APPENDIX

1. *Vapor pressure*
   The functional dependence of the vapour pressure (measured in Pa) of pure substances p_i^0 on temperature is generally available in the form of Antoine equation:

$$p_i^0 = \exp\left[A - \frac{B}{C+T}\right]$$

   T is expressed in K. A, B, and C are constant deduced by regression of experimental measurements (18). Data for few common substances are listed below:

   - Acetone: A = 16.6513, B = 2940.46, C = −35.93
   - Chloroform: A = 15.9732, B = 2696.79, C = −46.16
   - Ethanol: A = 18.9119, B = 3803.98, C = −41.68
   - Water: A = 18.3036, B = 3816.44, C = −46.13

2. *Surface tension of liquid in air*
   Data for few common substances are listed below (18):

   - Acetone: 0.024 N/m
   - Chloroform: 0.027 N/m
   - Ethanol: 0.023 N/m
   - Water: 0.073 N/m

   In the case of water-ethanol mixtures, the liquid surface tension γ_L(N/m) can be estimated by the following empirical relation (at 298 K):

$$\gamma_L = \frac{3.35 + 20.6x}{0.0465 + x} \cdot 10^{-3}$$

   where x is the mole fraction of ethanol (9).

3. *Water activity and activity coefficients*
   Water activities a_w of water-sugar mixtures at 25°C are fitted by the following polynomial correlation:

$$a_w = -0.27w^3 - 0.08w^2 - 0.09w + 1.00$$

   where w is the sugar weight fraction (156).
   For NaCl aqueous solutions, an empirical correlation between the water activity coefficient ξ_{water} and molar fraction of solute x_{NaCl} has been derived by Schofield (1989) as reported in (9):

$$\xi_{water} = 1 - 0.5x_{NaCl} - 10x_{NaCl}^2$$

   For aqueous solution of $CaCl_2$, in the range of mass fraction (w) 32.2–46.2 %, M. Courel (157) proposed the following empirical correlation for the water activity a_w in solution:

$$a_w = 1.6941 - 0.0410w_{CaCl_2} + 2.4 \cdot 10^{-4} w_{CaCl_2}^2$$

4. *Latent heat of vaporization*
   The enthalpy of saturated water vapour λ, reported in thermodynamic tables available in literature (19), can be deduced from the following equation (range of validity: 273–373 K):

$$\lambda(T) = 1.7535T + 2024.3$$

   where T is expressed in K, and λ in kJ/kg.

5. *Thermal conductivity*
   The following correlations allow to evaluate thermal conductivities of water vapour (k_{H_2O}) and air (k_{air}), of relevant interest in MD

applications (9):

$$k_{H_2O} = 2.72 \cdot 10^{-3} + 5.71 \cdot 10^{-5} T$$

$$k_{air} = 2.72 \cdot 10^{-3} T + 7.77 \cdot 10^{-5} T$$

The measured thermal conductivities at 296 K for some common hydrophobic polymers span in a relatively narrow range (158):

- Polypropylene (PP): $0.11-0.16\,\mathrm{W\,m^{-1}K^{-1}}$;
- Polyvinylidenedifluoride (PVDF): $0.17-0.19\,\mathrm{W\,m^{-1}K^{-1}}$;
- Polytetrafluoroethylene (PTFE): $0.25-0.27\,\mathrm{W\,m^{-1}K^{-1}}$.

REFERENCES

1. Stankiewicz, A. and Moulijn, J.A. (2002) Process Intensification. *Ind. Eng. Chem. Res.*, 41 (8)1996: 1920–1924.
2. Drioli, E. and Curcio, E. (2004) Perspectives for Membrane Contactors Application in Water Treatment. *J. Ind. Eng. Chem.*, 10 (1): 24–32.
3. Gabelman, A. and Hwang, S.-T. (1999) Hollow Fiber Membrane Contactors. *J. Membrane Sci.*, 159: 61–106.
4. Isetti, C., Nannei, E., and Magrini, A. (1997) On the Performance of an Air-Liquid Contactor for Air-Handling Applications. *Energy and Buildings*, 25: 185–193.
5. Rogers, J.D. and Long Jr. R.L., (1997) Modelling Hollow Fiber Membrane Contactors Using Film Theory, Voronoi Tessellations, and Facilitation Factors for Systems with Interface Reactions. *J. Membrane Sci.*, 134: 1–17.
6. Frank, G.T. and Sirkar, K.K. (1985) Alcohol Production by Yeast Fermentation and Membrane Extraction. *Biotech. Bioeng. Symp.*, 15: 621–631.
7. Hoq, M.M., Yamane, T., Shimizu, S., Funada, T., and Ishida, S. (1985) Continuous Hydrolysis of Olive Oil by Lipase in a Microporous Hydrophobic Membrane Bioreactor. *J. Am. Oil Chem. Soc.*, 62: 1016–1021.
8. Giorno, L., Li, N., and Drioli, E. (2003) Preparation of Oil-In-Water Emulsions Using Polyamide 10 kDa Hollow Fibre Membrane. *J. Membrane Sci.*, 217: 173–180.
9. Lawson, K.W. and Lloyd, D.R. (1997) Membrane Distillation. *J. Membrane Sci.*, 124: 1–25.
10. Hogan, P.A., Sudjito., Fane, G.A., and Morrison, G.L. (1991) Desalination by Solar Heated Membrane Distillation. *Desalination*, 81: 81–90.
11. Bouguecha, S. and Dhabhi, M. (2002) Fluidised Bed Crystalliser and Air Gap Membrane Distillation as a Solution to Geothermal Water Desalination. *Desalination*, 152: 237–244.
12. Hanafi, A. (1994) Desalination Using Renewable Energy Sources. *Desalination*, 97: 339–352.
13. de Andrés, M.C., Dria, J., Khayet, M., Pena, L., and Mengual, J.I. (1998) Coupling of a Membrane Distillation Module to a Multieffect Distiller for Pure Water Production. *Desalination*, 115: 71–81.

14. Curcio, E., Criscuoli, A., and Drioli, E. (2001) Membrane Crystallizers. *Ind. Eng Chem Res.*, 40 (12): 2679–2684.
15. Bodell, B.R. (1963) Silicone Rubber Vapour Diffusion in Saline Water Distillation. U.S. Patent 285,032.
16. Findley, M.E. (1967) Vaporization Through Porous Membranes. *Ind. Eng. Chem. Process Des. Dev.*, 6: 226–230.
17. Drioli, E., Jiao, B.L., and Calabrò, V. (1992) The Preliminary Study on the Concentration of Orange Juice by Membrane Distillation. *Proc. Int. Soc. Citriculture*, 3: 1140–1144.
18. Reid, R.C., Prausnitz, J.M., and Sherwood, T.K. (1977) *The Properties of Gases and Liquids*, 3rd ed.; McGraw-Hill: New York.
19. Perry, R.H. (1984) *Perry's Chemical Engineering Handbook*, 6th ed.; McGraw-Hill Book Co: Singapore.
20. Prausnitz, J.M. (1969) *Molecular Thermodynamics of Fluid-Phase Equilibria*. Prentice-Hall: Englewood Cliffs (NJ).
21. Sarti, G.C., Gostoli, C., and Bandini, S. (1993) Extraction of Organic Components from Aqueous Streams by Vacuum Membrane Distillation. *J. Membrane Sci.*, 80: 21–33.
22. Atkins, P.W. (1990) *Physical Chemistry*, 4th ed.; Oxford University Press: Oxford.
23. Laganà, F., Barbieri, G., and Drioli, E. (2000) Direct Contact Membrane Distillation: Modelling and Concentration Experiments. *J. Membrane Sci.*, 166: 1–11.
24. Gekas, V. and Hallstrom, B. (1987) Mass Transfer in the Membrane Concentration Polarization Layer Under Turbulent Cross Flow. I. Critical Literature Review and Adaptation of Existing Sherwood Correlations to Membrane Operations. *J. Membrane Sci.*, 30: 153–170.
25. Bennett, C. and Myers, J. (1982) *Momentum Heat, and Mass Transfer*. McGraw-Hill: New York.
26. Deissler, R. (1961) Analysis of Turbulent Heat Transfer, Mass Transfer and Friction in Smooth Tubes and High Prandtl and Schmidt Numbers. In *Advances in Heat and Mass Transfer*; Hartnett, J.P., ed.; McGraw-Hill: New York.
27. Notter, R.H. and Sleicher, C.A. (1971) The Eddy Diffusivity in the Turbulent Boundary Layer Near a Wall. *Chem. Eng. Sci.*, 26: 161–171.
28. Gilliland, E. and Sherwood, T. (1934) Diffusion of Vapors into an a Air Stream. *Ind. Eng. Chem.*, 26: 516–523.
29. Yang, M.C. and Cussler, E.L. (1986) Designing Hollow-Fiber Contactors. *AIChE J.*, 32: 1910–1915.
30. Wickramasinghe, S.R., Semmens, M.J., and Cussler, E.L. (1992) Mass Transfer in Various Hollow Fiber Geometries. *J. Membrane Sci.*, 69: 235–250.
31. Wang, K.L. and Cussler, E.L. (1993) Baffled Membrane Modules Made with Hollow Fiber Fabric. *J. Membrane Sci.*, 85: 265–278.
32. Bhaumik, D., Majumdar, S., and Sirkar, K.K. (1998) Absorption of CO_2 in a Transverse Flow Hollow Fiber Membrane Module Having a Few Wraps of the Fiber Mat. *J. Membrane Sci.*, 138: 77–82.
33. Fujii, Y., Kigoshi, S., Iwatani, H., and Aoyama, M. (1992) Selectivity and Characteristics of Direct Contact Membrane Distillation Type Experiment. I. Permeability and Selectivity Through Dried Hydrophobic Fine Porous Membranes. *J. Membrane Sci.*, 72: 53–72.

34. Kast, W. and Hohenthanner, C.-R. (2000) Mass Transfer Within the Gas-Phase of Porous Media. *Int. J. Heat and Mass Trans.*, 43: 807–823.
35. Kuhn, H. and Fostering, H.-D. (2000) *Principles of Physical Chemistry*. Wiley: New York.
36. Phattaranawik, J., Jiraratananon, R., and Fane, A.G. (2003) Effect of Pore Size Distribution and Air Flux on Mass Transport in Direct Contact Membrane Distillation. *J. Membrane Sci.*, 215: 75–85.
37. Mason, E.A. and Malinauskas, A.P. (1983) *Gas Transport in Porous Media: The Dusty-Gas Model*. Elsevier: New York.
38. Fane, A.G., Schofield, R.W., and Fell, C.J.D. (1987) The Efficient Use of Energy in Membrane Distillation. *Desalination*, 64: 231–243.
39. Schofield, R.W., Fane, A.G., and Fell, C.J.D. (1990) Gas and Vapour Transport through Microporous Membranes. II: Membrane Distillation. *J. Membrane Sci.*, 53: 173–185.
40. Bandini, S., Gostoli, C., and Sarti, G.C. (1992) Separation Efficiency in Vacuum Membrane Distillation. *J. Membrane Sci.*, 73: 217–229.
41. Bird, R.B., Stewart, W.E., and Lightfoot, E.N. (1960) *Transport Phenomena*. Wiley: New York.
42. Kimura, S. and Nakao, S. (1987) Transport Phenomena in Membrane Distillation. *J. Membrane Sci.*, 33: 285–298.
43. Schofield, R.W., Fane, A.G., and Fell, C.J.D. (1987) Heat and Mass Transfer in Membrane Distillation. *J. Membrane Sci.*, 33: 299–313.
44. Pena, L., Godino, M.P., and Mengual, J.I. (1998) A Method to Evaluate the Net Membrane Distillation Coefficient. *J. Membrane Sci.*, 143: 219–233.
45. Martinez, L. and Vazquez-Gonzalez, M.I. (2000) A Method to Evaluate Coefficients Affecting Flux in Membrane Distillation. *J. Membrane Sci.*, 173: 225–235.
46. Ugrozov, V.V. and Elkina, I.B. (2002) Mathematical Modeling of Influence of Porous Structure a Membrane on its Vapour-Conductivity in the Process of Membrane Distillation. *Desalination*, 147 (1–3): 167–171.
47. Gryta, M., Tomaszewska, M., and Morawski, A.W. (1997) Membrane Distillation with Laminar Flow. *Sep. Purif. Tech.*, 11: 93–101.
48. McCabe, W.L., Smith, J.C., and Harriot, P. (1985) *Unit Operations of Chemical Engineering*, 4th ed.; McGraw-Hill: New York.
49. Ozisik, M.N. (1985) *Heat Transfer*. McGraw-Hill: New York.
50. Gryta, M. and Tomaszewska, M. (1998) Heat Transport in the Membrane Distillation Process. *J. Membrane Sci.*, 144: 211–222.
51. Mengual, J.I., Khayet, M., and Godino, M.P. (2004) Heat and Mass Transfer in Vacuum Membrane Distillation. *Int. J. Heat and Mass Transfer*, 47: 865–875.
52. Bouguecha, S., Chouikh, R., and Dhahbi, M. (2002) Numerical Study of the Coupled Heat and Mass Transfer in Membrane Distillation. *Desalination*, 152: 245–252.
53. Martinez-Diez, L., Vasquez-Gonzalez, M.I., and Florido-Diaz, F.J. (1998) Study of Membrane Distillation Using Channel Spacers. *J. Membrane Sci.*, 144: 45–56.
54. Phattaranawik, J., Jiraratananon, R., and Fane, A.G. (2003) Effects of Net-Type Spacers on Heat and Mass Transfer in Direct Contact Membrane Distillation and Comparison with Ultrafiltration Studies. *J. Membrane Sci.*, 217: 193–206.
55. Phattaranawik, J., Jiraratananon, R., and Fane, A.G. (2003) Heat Transport and Membrane Distillation Coefficients in Direct Contact Membrane Distillation. *J. Membrane. Sci.*, 212: 177–193.

56. Martinez-Diez, L., Florido-Diaz, F.J., and Vasquez-Gonzalez, M.I. (1999) Study of Evaporation Efficiency in Membrane Distillation. *Desalination*, 126: 193–198.
57. Calabrò, V., Drioli, E., and Matera, F. (1991) Membrane Distillation in the Textile Wastewater Treatment. *Desalination*, 83 (1–3): 209–224.
58. Warner, S.B. (1995) *Fiber Science*. Prentice-Hall: Englewood Cliffs (NJ).
59. Jonsson, A.S., Wimmerstedt, R., and Harrysson, A.C. (1985) Membrane Distillation-A Theoretical Study of Evaporation through Microporous Membranes. *Desalination*, 56: 237–249.
60. Gostoli, C., Sarti, G.C., and Matulli, S. (1987) Low Temperature Distillation through Hydrophobic Membranes. *Sep. Sci. Tech.*, 22: 855–872.
61. Agashichev, S.D. and Falalejev, D.V. (1996) Modeling Temperature Polarization Phenomena for Longitudinal Shell-Side Flow in Membrane Distillation Process. *Desalination*, 108: 99–103.
62. Imdakm, A.O. and Matsuura, T. (2004) A Monte Carlo Simulation Model for Membrane Distillation Processes: Direct Contact (MD). *J. Membrane Sci.*, 237 (1/2): 51–59.
63. Mengual, J.I., Ortiz de Zarate, J., Pena, L., and Velazquez, A. (1993) Osmotic Distillation through Porous Hydrophobic Membranes. *J. Membrane Sci.*, 82: 129–140.
64. Celere, M. and Gostoli, C. (2002) The Heat and Mass Transfer Phenomena in Osmotic Membrane Distillation. *Desalination*, 147: 133–138.
65. Sheng, J. (1993) Osmotic Distillation Technology and its Applications. *Austral. Chem. Eng. Conf.*, 3: 429–432.
66. Kunz, W., Benhabiles, A., and Ben-Aim, R. (1996) Osmotic Evaporation through Macroporous Hydrophobic Membranes: A Survey of Current Research and Applications. *J. Membrane Sci.*, 121: 25–36.
67. Juby, G.J.G., Schutte, C.F., and Van Leeuwen, J. (1996) Desalination of Calcium Sulphate Scaling Mine Water. Design and Operation of the SPARRO Process. *Water SA.*, 22 (2): 161–172.
68. Sluys, J.T.M., Verdoes, D., and Hanemaaijer, J.H. (1996) Water treatment in a Membrane-Assisted Crystalliser (MAC). *Desalination*, 104: 135–139.
69. Garside, J., Mersmann, A., and Nyvlt, J. (2002) *Measurement of Crystal Growth and Nucleation Rates*. IChemE: Rugby, (UK).
70. Randolph, A.D. and Larson, M.A. (1988) *Theory of Particulate Processes, Analysis and Techniques of Continuous Crystallization*. Academic Press, Inc.: San Diego (CA).
71. Volmer, M. and Weber, A. (1926) Keimbildung in ubersattigten Gebilden. *Z. Phys. Chem.*, 119: 277–301.
72. Dirksen, J.A. and Ring, T.A. (1991) Fundamentals of Crystallization: Kinetic Effects on Particle Size Distribution and Morphology. *Chem. Eng. Sci.*, 46: 2389–2425.
73. Mulder, M. (1996) *Basic Principles of Membrane Technology*. Kluwer Academic Publishers: Dordrecht.
74. Lloyd, D.R., Kinzer, K.E., and Tseng, H.S. (1990) Microporous Membrane Formation via Thermally Induced Phase Separation. I. Solid–Liquid Phase Separation. *J. Membrane Sci.*, 52: 239–261.
75. Tomaszewska, M. (1996) Preparation and Properties of Flat-Sheet Membranes from Poly(vinylidene fluoride) for Membrane Distillation. *Desalination*, 104: 1–11.

76. Strathmann, H., Kock, K., Amar, P., and Baker, R.W. (1975) The Formation Mechanism of Asymmetric Membranes. *Desalination*, 16: 179–203.
77. Burgoyne, A. and Vahdati, M.M. (2000) Review. Direct Contact Membrane Distillation. *Sep. Science and Tech.*, 35 (8): 1257–1284.
78. Arcella, V., Colaianna, P., Maccone, P., Sanguinetti, A., Gordano, A., Clarizia, G., and Drioli, E. (1999) A Study on a Perfluoropolymer Purification and its Application to Membrane Formation. *J. Membrane Sci.*, 163: 203–209.
79. Wang, D., Li, K., and Teo, W.K. (2000) Porous PVDF Asymmetric Hollow Fiber Membranes Prepared with the Use of Small Molecular Additives. *J. Membrane Sci.*, 178: 13–23.
80. Feng, C., Shi, B., Li, G., and Wu, Y. (2004) Preliminary Research on Microporous Membranes F2.4 for Membrane Distillation. *Separation and Purification Technology*, 39: 221–228.
81. Xu, J.B., Lange, S., Bartley, J.P., and Johnson, R.A. (2004) Alginate-Coated Microporous PTFE Membranes for Use in the Osmotic Distillation of Oily Feeds. *J. Membrane Sci.*, 240: 81–89.
82. Favia, P. and D'Agostino, R. (1998) Plasma Treatments and Plasma Deposition of Polymers for Biomedical Applications. *Surface and Coatings Tech.*, 98: 1102–1106.
83. Kong, Y., Lin, X., Wu, Y., Chen, J., and Xu, J. (1992) Plasma Polymerisation of Octafluorocyclobutane and Hydrophobic Microporous Composite Membranes for Membrane Distillation. *J. Applied Polymer Sci.*, 46: 191–199.
84. Khayet, M. and Matsuura, T. (2003) Application of Surface Modifying Macromolecules for the Preparation of Membranes for Membrane Distillation. *Desalination*, 158: 51–56.
85. Keurentjes, J.T.F., Harbrecht, J.G., Brinkman, D., Hanemaaijer, M.A., Cohen Stuart, M.A., and van't Riet, K. (1989) Hydrophobicity Measurement of MF and UF Membranes. *J. Membrane Sci.*, 47: 333–344.
86. Zhang, W. and Hallstrom, B. (1990) Membrane Characterization by the Contact Angle Technique. I. Methodology of Captive Bubble Technique. *Desalination*, 79: 1–12.
87. Li, D. and Newmann, A.W. (1992) Equation of State for Interfacial Tensions of Solid-Liquid Systems. *Advances Coll. Interf. Sci.*, 39: 299–345.
88. Good, R.J. and van Oss, C.J. (1992) *Modern Approach to Wettability; The Modern Theory Contact Angle and the Hydrogen Bond Components of Surface Energies*; Schrader, M.E. and Loeb, G.L., eds.; Plenum Press: New York.
89. De Bartolo, L., Morelli, S., Bader, A., and Drioli, E. (2002) Evaluation of Cell Behaviour Related to Physico-Chemical Properties of Polymeric Membranes to be Used in Bioartificial Organs. *Biomaterials*, 23: 2485–2497.
90. Tomaszewska, M. (1999) Membrane Distillation. *Envir. Protect. Eng.*, 25 (1–2): 37–47.
91. Franken, A.C.M., Nolten, J.A.M., Mulder, M.H.V., Bargeman, D., and Smolders, C.A. (1987) Wetting Criteria for the Applicability of Membrane Distillation. *J. Membrane Sci.*, 33: 315–328.
92. Courel, M., Tronel-Peyroz, E., Rios, G.M., Dornier, M., and Reynes, M. (2001) The Problem of Membrane Characterization for the Process of Osmotic Distillation. *Desalination*, 140: 15–25.
93. Reed, B.W., Semmens, M.J., and Cussler, E.L. (1995) Membrane contactors. In *Membrane Separation Technology. Principles and Applications*; Noble, R.D. and Stern, S.A., eds.; Elsevier: Amsterdam.

94. Pena, L., Ortiz de Zarate, J.M., and Mengual, J.I. (1993) Steady States in Membrane Distillation: Influence of Membrane Wetting. *J. Chem. Soc. Faraday Trans.*, 89: 4333–4338.
95. Gostoli, C. and Sarti, G.C. (1989) Separation of Liquid Mixtures by Membrane Distillation. *J. Membrane Sci.*, 41: 211–224.
96. Schofield, R.W., Fane, A.G., and Fell, C.J.D. (1990) Gas and Vapour Transport through Microporous Membranes. I: Knudsen-Poiseuille Transition. *J. Membrane Sci.*, 53: 159–171.
97. Martinez-Diez, L. and Vazquez-Gonzalez, M.I. (1996) Temperature Polarization in Mass Transport through Microporous Membranes. *AIChE J.*, 42: 1844–1852.
98. Martinez, L., Florido-Diaz, F.J., Hernandez, A., and Pradanos, P. (2003) Estimation of Vapour Transfer Coefficient of Hydrophobic Porous Membranes for Applications in Membrane Distillation. *Separation and Purification Technology*, 33: 45–55.
99. Drioli, E. and Wu, Y. (1985) Membrane Distillation: An Experimental Study. *Desalination*, 53: 339–346.
100. Franken, A.C.M., Nolten, J.A.M., Mulder, M.H.V., and Smolders, C.A. (1987) Ethanol-Water Separation by Membrane Distillation: Effect of Temperature Polarization. In *Synthetic Polymeric Membranes*; Sedlacek, B. and Kahovec, J., eds.; Walter de Gruyter and Co.: New York.
101. Gryta, M. (2002) The Assessment of Microorganisms Growth in the Membrane Distillation System. *Desalination*, 142: 79–88.
102. Drioli, E., Wu, Y., and Calabrò, V. (1987) Membrane Distillation in the Treatment of Aqueous Solutions. *J. Membrane Sci.*, 33: 277–284.
103. Calabrò, V., Jiao, D.L., and Drioli, E. (1994) Theoretical and Experimental Study on Membrane Distillation in the Concentration of Orange Juice. *Ind. Eng. Chem. Res.*, 33: 1803–1808.
104. Durham, R.J. and Nguyen, M.H. (1994) Hydrophobic Membrane Evaluation and Cleaning for Osmotic Distillation of Tomato Puree. *J. Membrane Sci.*, 87: 181–189.
105. Udriot, H., Araque, A., and von Stockar, U. (1994) Azeotropic Mixtures May Be Broken by Membrane Distillation. *Chem. Eng. J.*, 54: 87–93.
106. Andersson, S.-I., Kjellander, N., and Rodesjo, B. (1985) Design and Field Tests of a New Membrane Distillation Desalination Process. *Desalination*, 56: 345–354.
107. Gore, D.W. (1982) Gore-Tex Membrane Distillation, *Proc. 10th Ann. Con. Water*, July 25–29, 1982 (Honolulu, Hawaii).
108. Koschikowski, J., Wieghaus, M., and Rommel, M. (2003) Solar Thermal-Driven Desalination Plants Based on Membrane Distillation. *Desalination*, 156: 295–304.
109. Schneider, K., Holz, W., Wollbeck, R., and Ripperger, S. (1988) Membranes and Modules for Transmembrane Distillation. *J. Membrane Sci.*, 39: 25–42.
110. Bellhouse, B.J., Costigan, G., Abhinava, K., and Merry, A. (2001) The Performance of Helical Screw-Thread Inserts in Tubular Membranes. *Sep. Pur. Technology*, 22/23: 89–113.
111. Ghogomu, J.N., Guigui, C., Rouch, J.C., Clifton, M.J., and Aptel, P. (1993) Hollow-Fibre Membrane Module Design: Comparison of Different Curved Geometries with Dean Vortices. *J. Membrane Sci.*, 81: 71–80.
112. Zhu, C. and Liu, G. (2000) Modelling of Ultrasonic Enhancement on Membrane Distillation. *J. Membrane Sci.*, 176: 31–41.

113. Lawson, K.W., Hall, M.S., and Lloyd, D.R. (1995) Compaction of Microporous Membranes Used in Membrane Distillation. I: Effect on Gas Permeability. *J. Membrane Sci.*, 101: 99–108.
114. Hambury, W.T. and Hodgkiess, T. (1985) Membrane Distillation—An Assessment. *Desalination*, 56: 287–297.
115. Kjellander, N. (1987) Design and Field Tests of a Membrane Desalination System for Seawater Desalination. *Desalination*, 61: 237–243.
116. Basini, L., D'Angelo, G., Gobbi, M., Sarti, G.C., and Gostoli, C. (1987) A Desalination Process Through Sweeping Gas Membrane Distillation. *Desalination*, 64: 231–243.
117. Godino, M.P., Pena, L., Rincon, C., and Mengual, J.I. (1996) Water Production from Brines by Membrane Distillation. *Desalination*, 108: 91–97.
118. Banat, F.A. and Simandl, J. (1998) Desalination by Membrane Distillation: A Parametric Study. *Sep. Sci. and Tech.*, 33 (2): 201–226.
119. Morrison, G.L., Fane, A.G., and Hogan, P. (1991) Solar Heated Membrane Distillation, *Proc. of 26th International Congress of ISES*, Denver.
120. Banat, F., Jumah, R., and Garaibeh, M. (2002) Exploitation of Solar Energy Collected by Solar Stills for Desalination by Membrane Distillation. *Renewable Energy*, 25: 293–305.
121. Lawson, K.W. and Lloyd, D.R. (1996) Membrane Distillation II. Direct Contact MD. *J. Membrane Sci.*, 120: 123–133.
122. Wirth, D. and Cabassud, C. (2002) Water Desalination Using Membrane Distillation: Comparison Between Inside/Out and Outside/In Permeation. *Desalination*, 147: 139–145.
123. Li, J.-M., Xu, Z.-K., Liu, Z.-M., Yuan, W.-F., Xiang, H., Wang, S.-Y., and Xu, Y.-Y. (2003) Microporous Polypropylene and Polyethylene Hollow Fiber Membranes. Part 3. Experimental Studies on Membrane Distillation for Desalination. *Desalination*, 155: 153–156.
124. Cabassud, C. and Wirth, D. (2003) Membrane Distillation for Water Desalination: How to Chose Appropriate Membranes. *Desalination*, 157: 307–314.
125. Martinez-Diez, L. and Florido-Diaz, F.J. (2001) Desalination of Brines by Membrane Distillation. *Desalination*, 137: 267–273.
126. Drioli, E., Laganà, F., Criscuoli, A., and Barbieri, G. (1999) Integrated Membrane Operations in Desalination Processes. *Desalination*, 122: 141–145.
127. Drioli, E., Criscuoli, A., and Curcio, E. (2002) Integrated Membrane Operations for Seawater Desalination. *Desalination*, 147: 77–81.
128. Criscuoli, A. and Drioli, E. (1999) Energetic and Exergetic Analysis of an Integrated Membrane Desalination System. *Desalination*, 124: 243–249.
129. Drioli, E., Curcio, E., Criscuoli, A., and Di Profio, G. (2004) Integrated System for Recovery of $CaCO_3$, NaCl and $MgSO_4 \cdot 7H_2O$ From Nanofiltration Retentate. *J. Membrane Sci.*, 239: 27–38.
130. Zolotarev, P.P., Ugrozof, V.V., Yolkina, I.B., and Nikulin, V.N. (1994) Treatment of Waste Water for Removing Heavy Metals by Membrane Distillation. *J. of Hazardous Mat.*, 37: 7–82.
131. Tomaszewska, M., Gryta, M., and Morawski, A.W. (2001) Recovery of Hydrocloric Acid from Metal Pickling Solutions by Membrane Distillation. *Sep. Purif. Tech.*, 22/23: 591–600.
132. Tomaszewska, M. (1993) Concentration of the Extraction Fluid From Sulphuric Acid Treatment of Phosphogypsum by Membrane Distillation. *J. Membrane Sci.*, 78: 277–282.

133. Zakrzewska-Trznadel, G., Harasimowicz, H., and Chmielewski, A.G. (1999) Concentration of Radioactive Components in Liquid Low-Level Radioactive Waste by Membrane Distillation. *J. Membrane Sci.*, 163: 257–264.
134. Zakrzewska-Trznadel, G., Chmielewski, A.G., and Miljevic, N.R. (1996) Separation of Protium/Deuterium and Oxygen-16/Oxygen-18 by Membrane Distillation. *J. Membrane Sci.*, 113: 337–342.
135. Gryta, M., Karakulski, K., and Morawski, A.W. (2001) Purification of Oily Wastewater by Hybrid UF/MD. *Water Res.*, 35 (15): 3665–3669.
136. Banat, F.A. and Simandl, J. (1996) Removal of Benzene Traces from Contaminated Water by Vacuum Membrane Distillation. *Chem. Eng. Sci.*, 51: 1257–1265.
137. Semmens, M.J., Qin, R., and Zander, A. (1989) Using a Microporous Hollow-Fiber Membrane to Separate VOCs From Water. *J. Am. Water Works Assoc.*, 81 (4): 162–167.
138. Urtiaga, A.M., Ruiz, G., and Ortiz, I. (2000) Kinetic Analysis of the Vacuum Membrane Distillation of Chloroform From Aqueous Solutions. *J. Membrane Sci.*, 165: 99–110.
139. Nene, S., Kaur, S., Sumod, K., Joshi, B., and Raghavarao, K.S.M.S. (2002) Membrane Distillation for the Concentration of Raw-Cane Sugar Syrup and Membrane Clarified Sugarcane Juice. *Desalination*, 147: 157–160.
140. Bandini, S. and Sarti, G.C. (2002) Concentration of Must Through Vacuum Membrane Distillation. *Desalination*, 149: 253–259.
141. Hogan, P.A., Canning, R.P., Peterson, P.A., Johnson, R.A., and Michaels, A.S. (1998) A New Option: Osmotic Distillation. *Chem. Eng. Prog.*, 94: 49–61.
142. Sirkar, K.K. (1997) Membrane Separation Technologies: Current Developments. *Chem. Eng. Comm.*, 157: 145–184.
143. Bailey, A.F.G., Barbe, A.M., Hogan, P.A., Johnson, R.A., and Sheng, J. (2000) Effect of Ultrafiltration on the Subsequent Concentration of Grape Juice by Osmotic Distillation. *J. Membrane Sci.*, 164: 195–204.
144. Cassano, A., Drioli, E., Galaverna, G., Marchelli, R., Di Silvestro, G., and Cagnasso, P. (2003) Clarification and Concentration of Fruit Juices by Integrated Membrane Processes. *J. Food Eng.*, 57: 153–163.
145. Sakai, K., Koyano, T., and Muroi, T. (1986) Effects of Temperature and Concentration Polarisation on Water Vapour Permeability for Blood in Membrane Distillation. *The Chem. Eng. J.*, 38: B33–B38.
146. Sakai, K., Muroi, T., Ozawa, K., Takesawa, S., Tamura, M., and Makane, T. (1986) Extraction of Solute-Free Water From Blood by Membrane Distillation. *Trans. Am. Soc. Artif. Intern. Org.*, 32: 397–400.
147. Capuano, A., Memoli, B., Andreucci, V.E., Criscuoli, A., and Drioli, E. (2000) Membrane Distillation of Human Plasma Ultrafiltrate and its Theoretical Applications to Haemodialysis Techniques. *Int. J. Artif. Org.*, 23 (7): 415–422.
148. Hoffmann, E., Pfenning, D.M., Philippsen, E., Schwahn, P., Sieber, M., When, R., and Woermann, D. (1987) Evaporation of Alcohol/Water Mixtures Through Hydrophobic Porous Membranes. *J. Membrane Sci.*, 34: 199–206.
149. Udriot, H., Ampuero, S., Marison, I.W., and von Stockar, U. (1989) Extractive Fermentation of Ethanol Using Membrane Distillation. *Biotechnology Letters*, 11 (7): 509–514.
150. Calibo, R.L., Matsumura, M., and Kataota, H. (1989) Continuous Ethanol Fermentation for Concentrated Sugar Solutions Coupled with Membrane Distillation Using a PTFE Module. *J. Ferment. & Bioeng.*, 67: 40–45.

151. Gryta, M., Morawski, A.W., and Tomaszewska, M. (2000) Ethanol Production in Membrane Distillation Bioreactor. *Catalysis Today*, 56: 159–165.
152. Banat, F.A. and Simandl, J. (1999) Membrane Distillation for Dilute Ethanol. Separation From Aqueous Streams. *J. Membrane Sci.*, 163: 333–348.
153. Curcio, E., Di Profio, G., and Drioli, E. (2003) Recovery of Fumaric Acid by Membrane Crystallization in the Production of L-malic Acid. *Sep. Purif. Tech.*, 33: 63–73.
154. Curcio, E., Di Profio, G., and Drioli, E. (2003) A New Membrane-Based Crystallization Technique: Tests on Lysozyme. *J. Crystal Growth*, 247: 166–176.
155. Di Profio, G., Curcio, E., Cassetta, A., Lamba, D., and Drioli, E. (2003) Membrane Crystallization of Lysozyme. Kinetic Aspects. *J. Crystal Growth*, 257: 359–369.
156. Catté, M., Dussap, C.-G., and Gros, J.-B. (1995) A Physical Chemical UNIFAC Model for Aqueous Solutions of Sugars. *Fluid Phase Equilibria*, 105: 1–25.
157. Courel, M. (1999) Etudes des transferts de matière en évaporation osmotique: application a la concentration des jus de fruits, PhD Thesis: University of Mompelier.
158. Brandrup, J. and Immergut, E.H. (1989) *Polymer Handbook*, 3rd ed.; Wiley: New York.